UNIVERSITY OF NAIROBI

SCHOOL OF PHYSICAL SCIENCES

CHARACTERIZATION OF Cu_2ZnSnS_4 (CZTS) THIN FILMS DEPOSITED BY POTENTIOSTATIC CZT ELEMENTAL DEPOSITION FOLLOWED BY CHEMICAL BATH IN SODIUM SULPHIDE SOLUTION

BY

JORIM OKOTH OBILA

I56/76308/2014

MSc. PHYSICS

DEPARTMENT OF PHYSICS

UNIVERSITY OF NAIROBI

A Thesis Submitted in Partial Fulfillment of the Requirements for Masters of Science Degree in Physics of the University of Nairobi

2016

DECLARATION

I declare that this thesis is my original work and has not been submitted elsewhere for examination. Where other people's work has been used, this has properly been acknowledged and referenced in accordance with the University of Nairobi's requirements

Jorim Okoth Obila
I56/76308/2014
Department of Physics
School of Physical Sciences
University of Nairobi

This thesis is submitted for examination with our approval as research supervisors:

Dr. Alex A. Ogacho
Department of Physics
University of Nairobi
P.O Box 30197-00100
Nairobi Kenya
ogachoa@uonbi.ac.ke

Dr. John O. Onyatta
Department of Chemistry
University of Nairobi
P.O Box 30197-00100
Nairobi Kenya
john.onyatta@uonbi.ac.ke

Dr. Marina Mukabi
Department of Chemistry
University of Nairobi
P.O Box 30197-00100
Nairobi Kenya
mmukabi@uonbi.ac.ke

ABSTRACT

Copper indium gallium selenide (CIGS) is currently one of the most efficient thin film solar technologies. However, the scarcity and toxicity of its primary constituents (that is indium/gallium) present a challenge for future large scale production and sustainability. Replacement of indium and gallium by earth abundant and nontoxic zinc and tin to form Cu_2ZnSnS_4 (CZTS) presents a viable alternative. In this work, CZTS thin films deposited by low cost electrodeposition coupled with chemical bath techniques at room temperature and then annealed under sulphur rich atmosphere were investigated. Redox potentials were investigated using a standard electrochemical cell with three electrodes: RE-Ag|AgCl (saturated KCl), CE-Pt wire and WE- TCO coated glass was used. The reduction potential of Cu^{2+}, Zn^{2+} and Sn^{4+} ions verses Ag/AgCl were, -0.47 V, -0.62 V and 0.63 V, respectively, verses Ag/AgCl. CZTS thin film quality determination was carried out using Raman spectroscopy which confirmed formation of quality CZTS film. Electrical characterization was carried out using four point probe instrument and the resistivity was in the order of $\sim 10^{-4}$ Ω-cm. The optical characterization was done using UV-VIS-NIR spectrophotometer. The band gaps of the annealed CZTS film ranged from 1.45 eV to 1.94 eV with absorption coefficient of order $\sim 10^4$ cm^{-1} in the visible and near infrared range of the solar spectrum.

Key words: Cu_2ZnSnS_4, stoichiometric, electrodeposition, chemical bath, reductionpotential

TABLE OF CONTENTS

DECLARATION ii
ABSTRACT iii
LIST OF FIGURES ix
LIST OF TABLES xiv
LIST OF ABBREVIATIONS xv
LIST OF SYMBOLS xvii
DEDICATION xviii
ACKNOWLEDGEMENTS xix

CHAPTER ONE: INTRODUCTION 1
1.1 Background 1
1.2 Statement of the Problem 4
1.3 Objectives 5
1.4 Justification 5
1.5 Significance of Study 5

CHAPTER TWO: LITERATURE REVIEW 7
2.1 Crystal Structure of Copper Zinc Tin Sulphide (CZTS) 7
2.2 Phases of CZTS 8
2.3 Electronic Properties of Cu_2ZnSnS_4 10
2.4 Preparation Method of Cu_2ZnSnS_4 Thin Film 10
2.5 Electrodeposition 10
2.6 Co-Deposition/Single Step-Electrodeposition 13
2.7 Chemical Bath Technique 13
2.8 Cu_2ZnSnS_4 Solar Cell Configuration 13

CHAPTER THREE: GENERAL THEORIES **15**
3.1 Optical Characterization 15
3.2 Electrical Characterization of CZTS 19
3.3 Defects in CZTS 20
3.4 Redox Potentialas of Cu, Zn and Sn metals 20
3.5 Determination of Quality of CZTS Film using Raman Spectroscopy 21

CHAPTER FOUR: MATERIALS AND METHODS **22**
4.1 Substrate preparation and cleaning 23
4.2 CZTS Thin Film Deposition 24
4.2.1 Deposition of CuS Thin Film 24
4.2.2 Deposition of ZnS Thin Film 24
4.2.3 Deposition of SnS Thin Film 25
4.3 Electrodeposition of CZTS 26
4.3.1 Preparation of the Solutions 26
4.3.2 Electrodeposition of CZT Thin Film 26
4.3.3 Layering Method 27
4.3.4 Co-electrodeposition Method 27
4.4 Chemical Bath (Deposition of Sulphur on the Deposited CZT) Sulfurization 28
4.5 Elemental Characterization of the CZT Deposited 28
4.6 Quality Determination of CZTS Film Formed 29
4.7 Optical and Electrical Characterization 30
4.8 Electrical Characterization 31

CHAPTER FIVE: RESULTS AND DISCUSSIONS 32
5.1 Cyclic and linear sweep voltammetry 32
5.1.0 Cyclic Voltammetry (CV) of Copper (Cu) 32
5.1.1 Cyclic Voltammetry of Zn 33
5.1.2 Cyclic Voltammetry of Sn 34

5.1.3 Cyclic Voltammetry of Zn and Cu 35
5.1.4 Cyclic Voltammetry of Cu, Zn and Sn 37
5.1.6 Linear sweep voltammetry of Sn 38
5.1.7 Linear sweep voltammetry of Cu and Zn 39
5.2 Co-electrodeposition of CZT 39
5.3 Elemental Analysis of the Deposited CZT 40
5.4 CuS Thin Film 42
5.4.1 Optical Properties of CuS Deposited by Electrodeposition Coupled with Chemical Bath Deposition 42
5.4.2 Reflectance and Transmittance of CuS 42
5.4.3 Band Gap of CuS 44
5.4.4 Quality Determination of CuS using Raman Spectroscopy 46
5.5 Optical Properties of ZnS Deposited by Electrodeposition Coupled with Chemical Bath Deposition 46
5.5.1 Reflectance and Transmittance of ZnS 46
5.5.2 Band Gap of Deposited ZnS 47
5.5.3 Quality Determination of ZnS using Raman Spectroscopy 48
5.6 Optical Properties of SnS Deposited by *SILAR* Method 49
5.6.1 Reflectance and Transmittance of SnS 49
5.6.2 Band Gap of SnS 50
5.7 Optical Properties of CZTS Deposited by Electrodeposition Coupled with Chemical Bath Technique 51
5.7.1 Optical Properties of As-Deposited CZTS Deposited by Layering Method 51
5.7.1.1 Band Gap of As-Prepared CZTS by Layering Method. 52
5.7.1.2 Optical Properties of Annealed CZTS Thin Film prepared by layering Method 52
5.7.1.3 Band Gap of CZTS after Annealing Thin Film Prepared by Layering Method 56

5.7.1.4 Absorption Coefficient of Annealed CZTS Film Deposited by Layering Method Followed by Chemical Bath in Na_2S Solution 58
5.7.1.5 Electrical Characterization of CZTS Film Deposited in Layers 59
5.7.1.6 Quality Determination of CZTS Film Deposited in Layers using Raman Spectroscopy 60
5.7.2 CZTS Film Deposited using co-electrodeposition of CZT Followed by Chemical Bath in Na_2S Solution 63
5.7.2.1 Optical properties of As-deposited CZTS Film deposited using co-electrodeposition of CZT followed by Chemical Bath in Na_2S Solution 63
5.6.2.2 Band Gap of As-deposited CZTS Film deposited using co-electrodeposition of CZT followed by Chemical Bath in Na_2S Solution 64
5.7.2.3 Optical Properties of Annealed CZTS Film Deposited Using Co-Electrodeposition of CZT followed by Chemical Bath in Na_2S Solution 65
5.7.2.4 Band Gap of Annealed CZTS Film Deposited using Co-electrodeposition of CZT followed by Chemical Bath in Na_2S Solution 66
5.7.2.5 Absorption Coefficient of CZTS Deposited using Co-electrodeposition of CZT followed by Chemical Bath in Na_2S Solution 68
5.7.2.6 Electrical Characterization of CZTS Deposited Using Co-electrodeposition of CZT followed by Chemical Bath in Na_2S Solution 69
5.7.2.7 Quality Determination of CZTS Film Deposited using Co-Electrodeposition of CZT followed by Chemical Bath in Na_2S Solution using Raman Spectroscopy 70
5.7.2.8 Summary of Raman peak shifts and band gaps of CZTS Film Deposited using Co-Electrodeposition of CZT followed by Chemical Bath in Na_2S Solution. 73
5.8 Comparison between CZTS Film Deposited in Layers and CZTS Deposited by Co-Electrodeposition 74

CHAPTER SIX: CONCLUSIONS AND RECCOMENDATIONS FOR FARTHER WORK 76
6.1 Conclusions 76
6.2 Recommendations for Farther Work 77

Reference 78

LIST OF FIGURES

Figure 1.1: The earth crust abundance of Cu, Zn, Ga, In and Sn 2
Figure 2.1: Evolution of CZTS structure. 7
Figure 2.2: (a) Kesterite structure and (b) Stannite structures. 8
Figure 2.3: Ternary phases in formation of Cu_2ZnSnS_4 9
Figure 2.4: The basics of electrodeposition setup. 12
Figure 2.5: A typical Cu_2ZnSnS_4 solar cell structure. 14
Figure 3.1: Presentation of band gap, E_g 15
Figure 3.2: Simple set up of 4 point probe system. 20
Figure 4.1: Summary of steps during substrate cleaning. Each step is coupled with ultrasonic cleaning with exception of the first and last step. 23
Figure 4.2: Summary of the *SILAR* process. 25
Figure 4.3: A block diagram for a typical experimental set-up for LIBS experiments. 29
Figure 4.4: A block diagram of major Raman spectroscopy components. 30
Figure 4.5: Photograph of *Shimadshu* UV-VIS-NIR spectrophotometer. 31
Figure 5.1: CV scans response of Cu electrodeposited on TCO glass electrode in solution containing 47 mM $CuSO_4.5H_2O$. Potential limit -1.00 V to 1.00 V, Scan rate 0.10 V/s, pH 3 and temperature of 23ºC. 32
Figure 5.2: CV scans response of Zn electrodeposited on TCO glass electrode in solution containing 450 mM $ZnSO_4.7H_2O$. Potential limit -1.00 V to 1.00 V, Scan rate 0.10 V/s, pH 3 and temperature of 40ºC. 34
Figure 5.3: CV scans response of Sn electrodeposited on TCO glass electrode in solution containing 260 mM $SnCl_4.5H_2O$. Potential limit -1.00 V to 0.00 V, Scan rate 0.10 V/s, pH 3 and temperature of 23ºC. 35
Figure 5.4: CV scans response of Cu and Zn electrodeposited on TCO glass electrode in solution containing a mixture of 47mM $CuSO_4.5H_2O$ and 450mM $ZnSO_4.7H_2O$. Potential limit -1.10 V to 0.80 V, Scan rate 0.10 V/s, pH 3 and temperature of 30ºC. 36

Figure 5.5: CV scans response of Cu, Sn and Zn electrodeposited on TCO glass electrode in solution containing 47 mM $CuSO_4.5H_2O$, 260mM $SnCl_4.5H_2O$ and 450mM $ZnSO_4.7H_2O$. Potential limit -1.00 V to 0.50 V, Scan rate 0.10 V/s, pH 3 and temperature of 27^oC.....38

Figure 5.6: Linear sweep scans response of Sn electrodeposited on TCO glass electrode in solution containing 260 mM $SnCl_4.5H_2O$. Potential limit 0.00 V to -1.00 V, Scan rate 0.10 V/s, pH 3 and temperature of 23^oC. 38

Figure 5.7: Linear sweep scans response of Cu and Zn electrodeposited on TCO glass electrode in solution containing a mixture of 47 mM $CuSO_4.5H_2O$ and 450 mM $ZnSO_4.7H_2O$. Potential limit -1.10 V to 0.80 V, Scan rate 0.10 V/s, pH 3 and temperature of 30^oC.....39

Figure 5.8: Current verses time for the co-electrodeposition of CZT at constant deposition potential of -1.20 V at room temperature. 47 mM of $CuSO_4.5H_2O$, 260 mM $SnCl_4.5H_2O$, 450 mM $ZnSO_4.7H_2O$, pH 3 and temperature 0f 30^oC.....40

Figure 5.9: Spectral lines of TCO coated glass. Energy 7.5 mJ, integration time 0.42 µS, shot counts 1, single count, Q switch delay time 150 µS and optical distance 3 mm.....41

Figure 5.10: Spectral lines of both the deposited CZT film and TCO coated glass. Energy 7.5mJ, integration time 0.42 µS, shot counts 1, single count, Q switch delay time 150 µS and optical distance 3 mm. 41

Figure 5.11: Spectral lines of deposited CZT film using LIBS spectroscopy. Energy 7.5 mJ, integration time 0.42 µS, shot counts 1, single count, Q switch delay time 150 µS and optical distance 3 mm. 42

Figure 5.12: Transmittance and Reflectance curves of CuS.....43

Figure 5.13: Band gap of CuS film (a) 36 nm, (b) 52 nm, (c) 79 nm, and (d). Variation of band gap with thickness for copper thin films.....45

Figure 5.14: Peaks of deposited CuS film. Laser 785 nm, exposure time 10 s, number of accumulations 5 s, objective ×50 and intensity 50%. 46

Figure 5.15: Transmittance and reflectance graphs of ZnS. 47

Figure 5.16: Band gap of deposited ZnS thin film.....48
Figure 5.17: Raman shifts of the deposited ZnS. Laser 785 nm, exposure time 10 s, number of accumulations 5 s, objective ×50 and intensity 50%. 48
Figure 5.18: Transmittance and reflectance of SnS deposited by *SILAR* technique.....49
Figure 5.19: (a) Direct,(b) indirect band gaps of as-deposited SnS.....50
Figure 5.20: Transmittance and reflectance of as-deposited CZTS deposited by layering method followed by chemical bath in Na_2S solution.(a) 130 nm, and (b) 250nm 51
Figure 5.21: Band gap of as-deposited CZTS deposited by layering method followed by chemical bath in Na_2S solution. (a) band gap of 250 nm and (b) band gap of 130 nm CZTS.....52
Figure 5.22: Transmittance and reflectance of CZTS deposited by layering method followed by chemical bath in Na_2S solution annealed at 450^oC. 53
Figure 5.23: Transmittance and reflectance of CZTS deposited by layering method followed by chemical bath in Na_2S solution annealed at 500^oC. 54
Figure 5.24: Transmittance and reflectance of CZTS deposited by layering method followed by chemical bath in Na_2S solution annealed at 550^oC 55
Figure 5.25: Band gap of CZTS deposited by layering method followed by chemical bath in Na_2S solution and annealed at: (a). 450^oC, (b) 500^oC (c) 550^oC and (d) the variation of band gap with annealing temperature.....56
Figure 5.26: The absorption coefficient of annealed CZTS deposited by layering method followed by chemical bath in Na_2S annealed at 550^oC.....58
Figure 5. 27: (a) Thickness variation with annealing temperature (b) Sheet resistivity variation with temperature.....59
Figure 5. 28: Raman peaks of CZTS film deposited by layering method followed by chemical bath in Na_2S solution annealed at 450^oC.Laser 785 nm, exposure time 10 s, number of accumulations 5 s, objective ×50 and intensity 50%.....60

Figure 5.29: Raman peaks of CZTS film deposited by layering method followed by chemical bath in Na_2S solution annealed at 500^oC. 61
Figure 5.30: Raman peaks of CZTS film deposited by layering method followed by chemical bath in Na_2S solution annealed at 550^oC. Laser 785 nm, exposure time 10 s, number of accumulations 5 s, objective ×50 and intensity 50%. 62
Figure 5.31: Transmittance and reflectance of as deposited CZTS deposited by use of co-electrodeposition of CZT followed by chemical bath in Na_2S. 63
Figure 5.32: Band gap of as-deposited CZTS deposited by use of co-electrodeposition of CZT followed by chemical bath in Na_2S.....64
Figure 5.33: Transmittance and reflectance of CZTS deposited by use of co-electrodeposition of CZT followed by chemical bath in Na_2S annealed at;(a) 450^oC, (b) 500^oC and (c) 550^oC. 65
Figure 5.34: Band gap of CZTS deposited by use of co-electrodeposition of CZT followed by chemical bath in Na_2S annealed at; (a) 450^oC, (b) 500^oC and (c) 550^oC.....67
Figure 5.35: Absorption coefficient variation with photon energy.....69
Figure 5.36: (a) Thickness variation with annealing temperature (b) Sheet resistivity variation with temperature. 70
Figure 5.37: Raman peaks of CZTS deposited by Co-electrodeposition method followed by chemical bath in Na_2S solution annealed at 450^oC. Laser 785 nm, exposure time 10 s, number of accumulations 5 s, objective ×50 and intensity 50%. 71
Figure 5.38: Raman peaks of CZTS deposited by Co-electrodeposition method followed by chemical bath in Na_2S solution annealed at 500^oC. Laser 785 nm, exposure time 10 s, number of accumulations 5 s, objective ×50 and intensity 50%. 72
Figure 5.39: Raman peaks of CZTS deposited by Co-electrodeposition method followed by chemical bath in Na_2S solution annealed at 550^oC. Laser

785 nm, exposure time 10 s, number of accumulations 5 s, objective ×50 and intensity 50%. 73

LIST OF TABLES

Table 5.1: Variation of film thickness, sheet resistivity and volume resistivity with temperature. 59

Table 5.2: Summary of variation of film thickness, sheet resistivity and volume resistivity with temperature..... 69

Table 5.3: Effect of annealing temperature on the Raman peaks and optical band gaps of the deposited CZTS films..... 73

Table 5.4: Comparison of the properties of CZTS film deposited in layers and that deposited by co-electrodeposition followed by chemical bath 74

LIST OF ABBREVIATIONS

E_{ex} and E_{ez} - Cross-over potentials

CdTe- Cadmium Telluride

CE- Counter electrode

CIGS- Copper Indium Gallium Selenide

Cu- Copper

CuS- Copper sulphide

CV- Cyclic voltammetry

CZTS- Copper Zinc Tin Sulphur

KCl- Potassium chloride

KCN- Potassium Cyanide

LIBS-Laser induced breakdown spectroscopy

N_2- Nitrogen gas

PD-KS- Partially Disordered Kesterite

RE- Reference electrode

S- Sulphur

SILAR- Successive ion layer adsorption and reaction

Sn- Tin

SnS- Tin sulphide

TCO- Transparent conducting oxide

UV-VIS-NIR- Ultraviolet - Visible - Near Infrared Rays

WE- Working electrode

Zn- Zinc

ZnS- Zinc sulphide

Ω-Ohm

LIST OF SYMBOLS

Symbol	Quantity	Units
A	Area	cm^2
α	Absorption coefficient	cm^{-1}
E_g	Band gap	eV
hv	Photon energy	eV
I	Light intensity	$Js^{-1}cm^{-2}eV^{-1}$
λ	Wavelength	nm

DEDICATION

This work is dedicated to Mealer Achieng'

and Immaculate Achieng'

.

ACKNOWLEDGEMENTS

I give special thanks to God for His faithfulness throughout the study period I had in the University of Nairobi. I thank University of Nairobi for the scholarship that has enabled me complete my Masters successfully and smoothly.

Much appreciation to Dr. Alex A. Ogacho for his generous support towards the success of this study, he ensured that I fully register as an MSc student in the university. His diverse practical knowledge in the laboratory really helped me a lot in completing my laboratory work at the right time. I take this special moment to appreciate Dr. Marina Mukabi and Dr. John Onyatta for ensuring the success of this work.

CHAPTER ONE: INTRODUCTION

1.1 BACKGROUND

Energy shortage has increased due to rapid population increase over years. This problem has resulted in low economic development and survival problems, for example; people in the rural cannot have enough energy to cook, do their laundry or light their houses effectively. Primarily energy consumption is from wood fuel and fossil fuels, which include oil, natural gas and coal. The consumption of fossil fuels has increased at an alarming rate, indicating that globally we are running out of low cost energy sources and in addition, the continued emission of carbon (IV) oxide from these sources is becoming a threat to humans and animals. This calls for need to change from fossil fuels to more sustainable energy sources. The non-fossil energy sources such as geothermal energy, nuclear energy, also have problems i.e. in geothermal energy, nuclear fission and nuclear fusion the problem of uncertain technology and economics for fusion and dry-rock geothermal (Holdren, 1991) is a major challenge. These kinds of non-fossil energy sources are not best option in addressing the problem of energy security, energy equity and environmental sustainability. The only source of energy that can fully address these three problems is solar energy since it is abundant and accessible by both the rural and urban population. In addition, it is environmentally friendly unlike other non-fossil sources of energy. Therefore cost of solar panels needs to be reduced so that most people can afford it for maximum solar energy harvest. This deserves research hence the need to conduct research on thin film solar cells technology.

The main thin film solar technology currently available include the amorphous silicon thin film which is expensive to manufacture because it requires a lot of skills and technology to make the silicon wafers thin enough. Other thin film solar cells include: copper indium selenide (CIS), cadmium telluride (CdTe), copper indium gallium selenide (CIGS), gallium arsenide (GAS) and copper zinc tin sulphide (Cu_2ZnSnS_4). Gallium arsenide and cadmium telluride contain toxic tellurium and arsenic elements, and copper indium gallium selenide system contains scarce indium elements. Figure 1.1 is showing earth crust abundance of Cu, Zn, Ga, In and Sn.

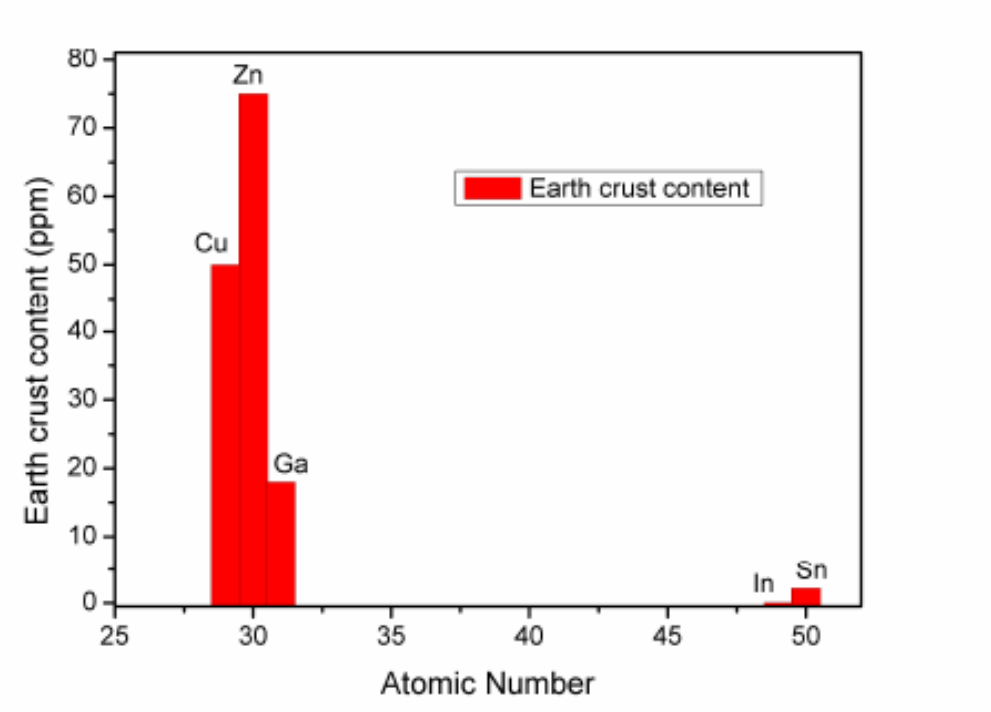

Figure 1.1: The earth crust abundance of Cu, Zn, Ga, In and Sn (adapted from Wang and Bell, 2011).

Due to factors stated above, these kinds of solar technology cannot be sustainable over a long period of time since there will be no or less raw materials making the technology extremely expensive. In Cu_2ZnSnS_4 (CZTS) solar technology, CZTS contain abundant, non-toxic and environmentally friendly elements i.e. Cu, Zn, Sn and S. CZTS is an environmentally safe form of CIGS with the rear indium and gallium replaced with the abundant Zinc and Tin and the environmentally unsafe selenium replaced with sulphur. CZTS is a quaternary compound of either stannite structure (Song *et al.*, 2014) or kesterite structure (Vasekar and Dhakal, 2013), which is mostly used in solar cells as an absorber layer. CZTS usually appears in kesterite phase since it is more stable thermodynamically in this phase as compared to stannite structure (Wang, 2011). CTZS acts as an absorber layer due to its high absorption coefficient of $\sim 10^4$ cm^{-1}. CZTS has a reported band gap range of 1.45 - 1.60 eV (Ahmed *et al.*, 2011). This is very close to optimal band gap of 1.35 eV, for thin film semiconductor for high efficient solar cells (Mkawi *et al*., 2013). This band range enables CZTS thin film to absorb

light in the visible and near infrared region of the solar spectrum especially the visible range which is rich in solar insolation.

Friedlmeier *et al.* in (1997) first reported an efficiency of 2.3% CZTS heterojunction (Wang, 2011). More studies have been done to develop this material as an absorber layer. These studies have seen the efficiency of CZTS solar technology improve over time. This has been seen since 2005 where the efficiency increased to 5.45% by optimization of sulfurization process (Wang, 2011). In 2008 an efficiency of 6.7% was reported (Katagiri *et al.*, 2008). In 2011 an efficiency of 8.4% was reported (Hiroi *et al.*, 2011). In 2012 an efficiency of 9.2% was achieved (Kato *et al.*, 2012). The current world record efficiency of CTZS stands at 12.6% (Wang, 2011). Despite the 12.6% efficiency achievement, this material continues to attract more attention and hence more research work need to be done on it. This is because of high efficiency of 30% predicted theoretically according to photon balance calculations of Shockley-Queisser (Mkawi *et al.*, 2013).

CZTS thin film deposition consists of low temperature film deposition followed by high temperature treatment. The film deposition has been done by vacuum and non-vacuum based methods. Originally CZTS nanocrystals was synthesized by non-vacuum based method by hot injection of a solution of elemental sulphur in oleylamine into a solution containing 1.5 mM of copper (II) acetylacetonate and 0.75 mM of tin (IV) bis (cacetylacetonate) dibromide in oleylamine at 225^{o}C (Zhou *et al*., 2013). CZTS has also been synthesized through solid state chemical reaction between ZnS, Cu_2S and SnS_2 but a single-phase CZTS only forms in small regions (Wang, 2011). Other non-vacuum methods include spray pyrolysis, electrochemical deposition, and successive ionic layer adsorption and reaction (*SILAR)* technique. Non-vacuum technique has a higher deposition rate (Wang, 2011) as compared to vacuum based methods. In vacuum-based deposition method, fabrication techniques involve deposition of CZTS thin film on a substrate by sputtering or evaporation of target sources under a specified pressure and temperature.

In this research electrochemical deposition method and chemical bath deposition techniques were combined to deposit CZTS. This was the first attempt of the combination of the two

methods to generate CZTS thin film. Electrochemical deposition has a number of advantages (Mkawi*et al.*, 2013), these include:

- High deposition rates of material of interest.
- It is cheap due to cheaper equipment
- The precursor solutions or starting materials need not to be pure as in vacuum deposition techniques.
- Film properties e.g. morphology and thickness can be controlled by varying electrochemical parameters e.g. temperature, current and potential.

Chemical bath technique also has a number of advantages:-

- Requires cheaper equipment
- Deposition rate can be varied by varying deposition conditions e.g. temperature, pH, duration of deposition etc.
- Deposition rate is also high

Due to these advantages electrochemical and chemical bath method were used to synthesize CZTS thin film. The thin film formed was analyzed for its quality, electrical and optical properties.

1.2 Statement of the Problem

Thin film technology is attracting more attention in photovoltaic applications specifically solar technology for large scale production with minimal material utilization. The most efficient thin film solar cell uses CIGS technology, which contains rare earth materials like indium and gallium which are expensive and toxic. Due to these reasons materials which are non-toxic and earthly abundant are deemed best for sustainable solar energy production. Attempts have been made to replace In, Ga with earth abundant materials like Zn and Sn to fabricate CZTS solar cells. However the efficiencies of CZTS solar cells are still very low compared to CIGS. The most probable reason being the difficulty of fabricating a quality CZTS which is free of defects. A number of techniques have been tested and various results

obtained. In this research, low cost technique comprising of electrodeposition and chemical bath have been used to achieve a quality CZTS film.

1.3 Objectives

The main objective was to deposit quality CZTS thin films by use of electrodeposition and chemical bath technique to develop low cost solar cell absorber layer.

Specific objectives

i. To evaluate the electrical and optical properties of CZTS thin films deposited by cathodic sweep electro-deposition coupled with chemical bath deposition techniques.
ii. To evaluate the effect of annealing temperature on CZTS thin films optical and electrical properties.
iii. To determine the quality of the deposited CZTS using Raman spectrophotometer.

1.4 Justification

The elements of the CZTS compound are abundant and non-toxic making them affordable and environmentally safe. Furthermore, the method used to deposit CZTS film which was the combination of electrodeposition and chemical bath technique is cheap and does not require much energy. Hence CZTS film deposited in this manner is the best option in making low cost solar cells.

1.5 Significance of Study

CIGS and CdTe are the two main thin film solar cells currently in use. Though these kinds of solar cells have experienced a large success in cost reduction, they contain indium and Tellurium which are rare and toxic. Therefore as use of solar panels spreads the availability of these materials pose the greatest challenge. In addition, CIGS and CdTe have reached their optimal efficiency level (Kanuru *et al.*, 2014) calling for research in other alternative materials to manufacture solar cells.

Since CZTS film can be used to replace CIGS film as an absorber layer in solar cells it becomes the best option for the thin film solar cells. The methods of production of CZTS thin films are less expensive as compared to those of producing CIGS thin films. And the most

outstanding advantage is that it contains earthly abundant materials. This shows that no matter how solar use spreads the manufacturers will not run out of materials. Moreover, the CZTS elements are non-toxic and therefore environmentally safe. Hence solar cells made from CZTS will be low cost and easily sustainable.

CHAPTER TWO: LITERATURE REVIEW

2.1 Crystal Structure of Copper Zinc Tin Sulphide (CZTS)

CZTS is a quaternary compound I_2-II-IV-VI_4 obtained through $CuInS_2$ chalcopyrite structure by substituting one-half of the constituent indium atoms with zinc and other half with tin, as shown in Figure 2.1. Indium is a group III transition element whereas zinc and tin are transition elements of group II and IV respectively.

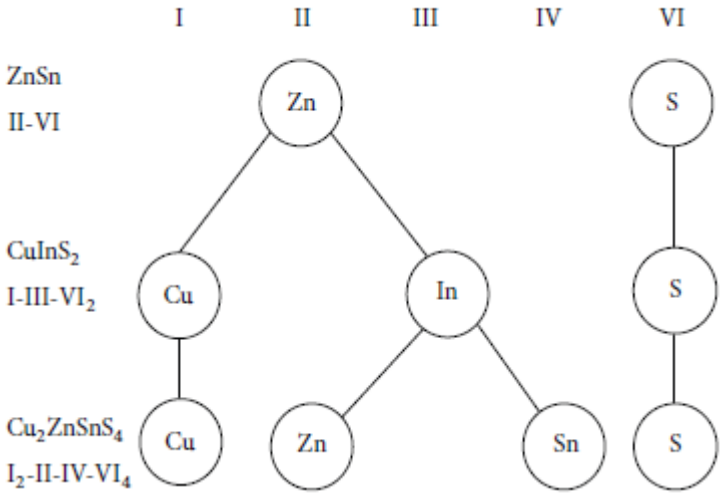

Figure 2.1: Evolution of CZTS structure (Song *et al*, 2013).

The structure of Cu_2ZnSnS_4 is still under contention with researchers not agreeing to a specific structure. It is however, believed that the structure of Cu_2ZnSnS_4 can be either stannite (Song *et al.*, 2014) or kesterite structure (Vasekar and Dhakal, 2013). The two structures at times exist simultaneously in Cu_2ZnSnS_4 since the energy difference between them is very small, about 3 meV/atom (Chen *et al.*, 2009). From experiments it has been shown that partially disordered kesterite (PD-KS) structure can exist, in which the atoms in the Cu+Zn (001) layer in the kesterite structure are disordered, while atoms in the Cu+Sn layer reside in the original position (Chen *et al.*, 2009). PD-KS has a higher energy than stannite structure because it does not obey the octet rule but it has a similar crystallographic patterning. Due to similar crystallographic patterning some experiments have confused the

two structures (Scragg, 2011). By first principle it has been proved that I_2-II-IV-VI_4 compounds are more stable in kesterite form because in kesterite structure the strain energy is lower than that of stannite structure (Chen *et al.*, 2009). Cu_2ZnSnS_4 has a stannite structure or kesterite structure depending on different locations of copper and zinc on the compound's structure as illustrated in Figure 2.2 (a) and (b).

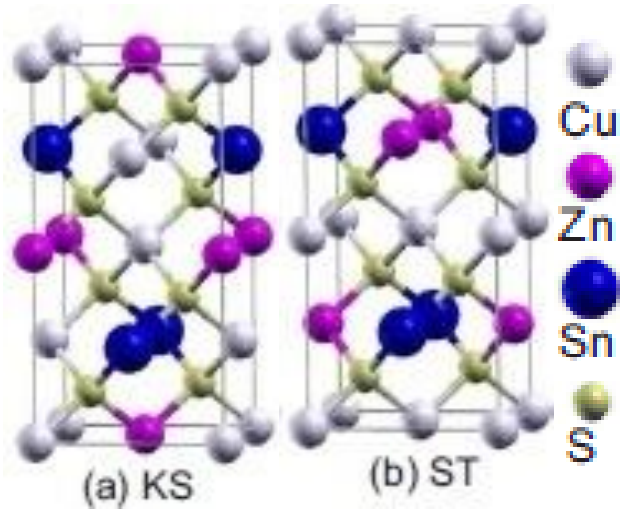

Figure 2.2: (a) Kesterite structure and (b) Stannite structures. (Chen *et al.*, 2009).

Structure of CZTS can be determined by simple crystal x-ray diffraction (Song *et al.*, 2014) but it is not easy to distinguish between CZTS kesterite or stannite structure using this method because XRD peaks of kesterite structure are similar to that of stannite structure. Neutron scattering has been used to differentiate between these structures.

2.2 Phases of CZTS

CZTS can be synthesized by solid state reaction between Cu_2S, ZnS and SnS_2. The CZTS quaternary phase is difficult to attain unlike the binary phases due to the four elements involved in its formation. In synthesizing quaternary phase, compositions of specific compounds need to be taken into consideration to avoid formation of binary phases and ternary impurity phases (Guo *et al.*, 2014).

No clear growth mechanism of Cu_2ZnSnS_4 has been reported yet this has made fabrication of single-phase Cu_2ZnSnS_4 to be difficult experimentally. Both theoretical and experimental

efforts have shown that the formation of CZTS system single-phase stannite Cu_2ZnSnS_4 exists only in a small region as shown below (Just *et al.*, 2011).

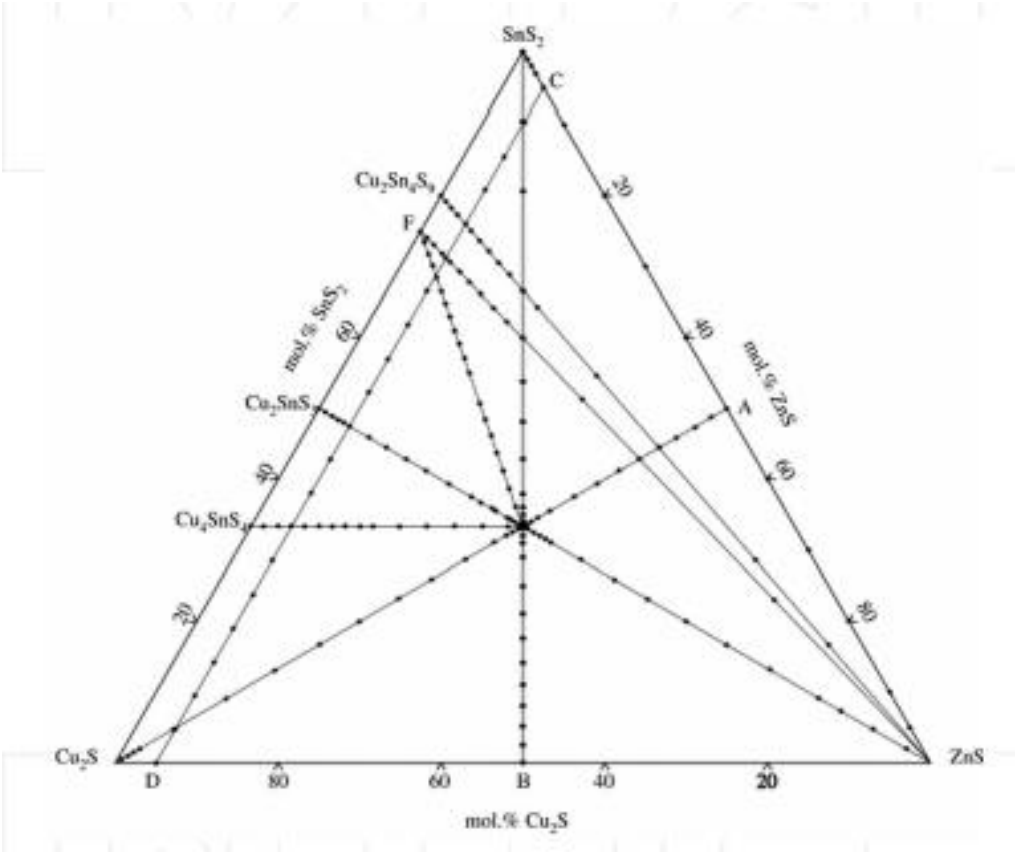

Figure 2.3: Ternary phases in formation of Cu_2ZnSnS_4 (Vasekar and Dhakal, 2013).

Figure 2.3 shows that the scope of chemical potential which favour synthesis of Cu_2ZnSnS_4 quaternary semiconductor phase is very narrow. Quaternary phase of Cu_2ZnSnS_4 can be obtained if Cu_2ZnSnS_4 as-prepared is annealed at a temperature over 350^oC (Mau and Kim, 2012). At this temperature (350^oC) different phases can be formed e.g. ZnS, Cu_3SnS_4. The crystal structures of Cu_2ZnSnS_4 and ZnS have similar lattice constants and their X-ray diffraction patterns overlap. Therefore to identify the extra phases in Cu_2ZnSnS_4, Raman Spectroscopy is used since the peaks of Cu_2ZnSnS_4 and its phases will not overlap (Shin *et al.*, 2011). ZnS binary phase has a larger band gap than Cu_2ZnSnS_4thatwill lead to formation of internal barriers which degrades the solar cells made from Cu_2ZnSnS_4 absorber layer.

Therefore a higher temperature of 500ºC is needed to get rid of ZnS binary phase completely since it is volatile at such temperatures. High temperature treatments result in increased crystallinity and increase in grain size. The crystallinity and the growth of large grain sizes at high temperature are achieved by annealing in $Ar+H_2S$. This is known as sulphurization and it helps in improving Cu_2ZnSnS_4 solar cells efficiencies. The maximum efficiency of Cu_2ZnSnS_4 solar cells is obtained in Zn-rich and Cu-poor materials. This prevents formation of degrading phases such as Cu-S and Cu-Sn-S.

2.3 Electronic Properties of Cu_2ZnSnS_4

Cu_2ZnSnS_4 has a band gap of 1.50 eV which is very good for solar applications since it is close to optimum band gap of 1.35 eV, which enables absorb solar radiation energy in the visible region which rich in solar insulation (Ananthan and Mahalaksmi, 2014). This increases the efficiency of CZTS thin film solar cells. This has made Cu_2ZnSnS_4 the best replacement for CIGS and CdTe in solar applications. Though the band gap is close to 1.35 eV, Cu_2ZnSnS_4 still has a low efficiency because of the phases involved and also not enough research has been directed towards it (Song *et al.,* 2014). Cu_2ZnSnS_4 has not been commercialized yet due to lack of enough information about it.

2.4 Preparation Method of Cu_2ZnSnS_4 Thin Film

Methods for Cu_2ZnSnS_4 thin film deposition include: atom beam sputtering, electron-beam-evaporated precursors, photo-chemical deposition, spray pyrolysis, hybrid sputtering, radio frequency magnetism sputtering, *SILAR* technique, and electrochemical deposition technique. Though there are a number of methods of preparing Cu_2ZnSnS_4 (Song *et al.,* 2014*)* thin films, this study concentrates only on electrochemical/electro-deposition combined with chemical bath technique. Since this is the method of interest in this research to produce a quality CZTS thin film in which the elements are stoichiometrically mixed.

2.5 Electrodeposition

The process of electrodeposition began in 1970s to fabricate Cu_2ZnSnS_4 absorber layer (Song *et al,* 2014*).* The efficiency of Cu_2ZnSnS_4 solar cells made by this method has increased over the years. In 2008 the efficiency was 0.8% (Scragg *et al.,* 2008), the efficiency improved to

3.4% in 2011 (Wang 2011). According to Song *et al*., (2013) electro-deposition is a coating method used to reduce the cations in the aqueous solution, or dip fluid in the cathode by supplying potential difference with external circuit. Generally, the basics of electrodeposition include; an electrolyte containing the desired ions to be deposited, a working electrode or substrate where deposition will take place, a counter electrode (inert as Pt), reference electrode e.g. Ag/AgCl and a potentiostat or galvanostat as a power source as shown in Figure 2.4. When a potential is applied, current flows through the electrolyte and the cations and anions move toward the working and counter electrodes respectively. Deposition occurs on the working electrode after undergoing some charge transfer. During deposition at the electrode, several reaction steps are involved (Septina, 2013):

i. Ionic transfer
ii. Discharge
iii. Breaking up of ion-ligand bond
iv. Incorporation of adatoms onto the electrode followed by nucleation and growth

Electrodeposition has been widely used in both research and industrial community to deposit thin film absorber layer such as CdTe and CIGS films (Wang and Bell, 2010). In using electro-deposition, the produced Cu/Zn/Sn is covered with sulfur and annealed in argon gas environment or it is simply annealed in $Ar+H_2S$ gases. In this research the made Cu/Zn/Sn is dipped into sodium sulphide solutions for sulphur adsorption.

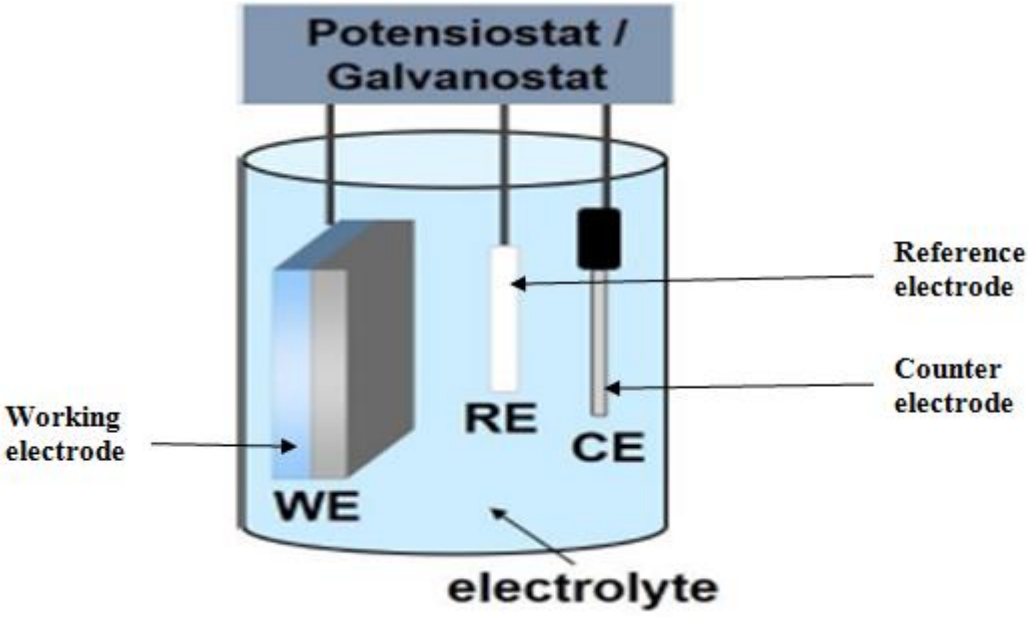

Figure 2.4: The basics of electrodeposition setup (Septina, 2013).

Electrodeposition has several advantages, which include:

- Environmentally safe
- Large area deposition
- High deposition rates of material of interest
- It is cheap due to cheaper equipment, does not require sophisticated high vacuum and high power supplies or high reaction temperature.
- The precursor solutions or starting materials need not to be pure as in vacuum deposition techniques
- Film properties e.g. morphology and thickness can be controlled by varying electrochemical parameters such as temperature, current and potential.
- Room temperature growth
- Less or almost no materials wastage
- Produces uniform coating

There are three ways in which the metals can be deposited by electrodeposition (Scragg, 2011):

I. Direct compound deposition

II. Co-deposition of mixed alloy Cu, Sn and Zn, which is of interest in this research

III. Sequential layer deposition of Cu, Sn and Zn

2.6 Co-Deposition/Single Step-Electrodeposition

In single stepelectrodeposition all of the required elements are deposited at once using a common electrolyte to produce a uniformly mixed precursor film. Here an electrolyte containing all the required ions is used to deposit the thin film on the working electrode. In Cu_2ZnSnS_4 thin film deposition an electrolyte containing Cu^{2+}, Zn^{2+} and Sn^{4+} is used followed by heat treatment at high temperature under Argon or sulfur to obtain the desired materials with high crystallinity.

In co-deposition method the film formed is homogeneously mixed and more uniform. The main challenge is deciding on the optimal potential to synthesize CZTS film (Septina *et al.*, 2013). This is because different metals are reduced at different potentials and condition of formation of each metal layer is very different. This can be solved by adjusting the electrolyte conditions.

2.7 Chemical Bath Technique

Chemical bath technique can be used to grow films on either metallic or non-metallic substrates by dipping them in appropriate solutions of metal salts without the application of any electric field (Mane and Lokhande, 2000).

2.8 Cu_2ZnSnS_4 Solar Cell Configuration

A typical Cu_2ZnSnS_4 solar cell has a structural arrangement of SLG/Mo/CZTS/ n-CdS/i-ZnO/n-ZnO structure, Figure 2.5. In this kind of cell molybdenum layer is used as a back contact since it is stable in harsh reactive conditions such as sulfur containing vapor and high temperatures. It is sputter-deposited on the glass substrate. The absorber layer CZTS which is a p-type semiconductor is then coated on the molybdenum layer. An n-CdS is then coated on the CZTS layer for the formation of p-n junction. Intrinsic ZnO (i-ZnO) is sputtering-coated on n-CdS to prevent its leakage. Transparent conducting oxide (TCO) is then deposited on i-

ZnO to front contact of CZTS solar cell. To measure the current-voltage (I-V) property of the cell, Ni/Al grid is deposited on both TCO and Mo layer (Jiang and Yang, 2013).

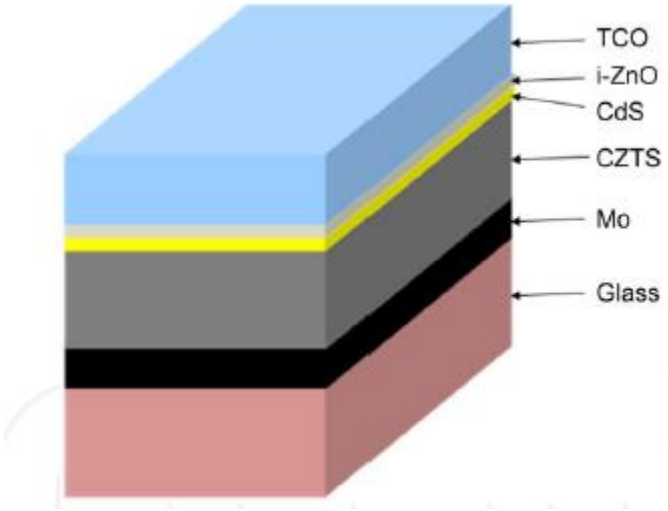

Figure 2.5: A typical Cu_2ZnSnS_4 solar cell structure (Jiang and Yang, 2013).

CHAPTER THREE: GENERAL THEORIES

3.1 Optical Characterization

i). Optical Absorption

The energy at which absorption starts is a characteristic for each material, it corresponds to direct band gap of CZTS. The optical absorption data is analyzed as follows (Pawar *et al*., 2011):

$$\alpha = \frac{A\left(h\nu - E_g\right)^n}{h\nu} \tag{3.1}$$

Where E_g is the band gap, α is the absorption coefficient, n is a constant and $h\nu$ is the photon energy, n takes the values of can be $1/2, 3/2$, 2 and 3 depending on the probability of transition. $1/2, 3/2$, 2 and 3 values is for direct forbidden, indirect allowed and indirect forbidden transitions, respectively. The transition is allowed if the plot of $(\alpha h\nu)^2$ verses $(h\nu)$ is linear.

ii). Optical band gap of CZTS film

Band gap is the energy difference between the top of valence band and bottom of the conduction band. This is indicated in Figure 3.1 by E_g.

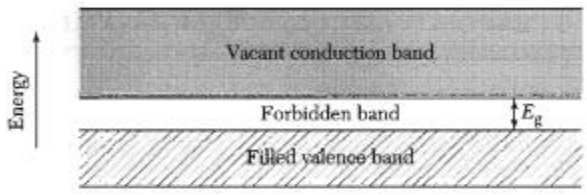

Figure 3.1: Presentation of band gap, E_g (Kittel, 2005)

The optical band gap of kesterite CZTS has theoretically been estimated to be 1.5 eV (Jiang and Yang, 2013). Experiments have shown that the band gap of CZTS film ranges from 1.4 -

1.5 eV confirming the theoretical result (Ahmed *et al.*, 2011). Experimentally the band gap can be obtained by use of reflectance and transmittance measurements as shown in equation (3.2).

Band gaps in semiconductor can be determined by using a graph of $(\alpha hv)^n$ versus hv, using equation (3.1). Where α is the absorption coefficient given by (Rahmani *et al.*, 2009);

$$\alpha = -\frac{1}{d}\ln\left(\frac{R_{normalized}}{1-T_{normalized}}\right) \tag{3.2}$$

Where, d is the film thickness, $R_{normalized}$ and $T_{normalized}$ are transmittance and reflectance of the film normalized, respectively.

And hv, the energy of incident photon given by,

$$E(eV) = \frac{1240}{\lambda(nm)} \tag{3.3}$$

λ, is the wavelength of incident photon.

E, is the energy (eV)

Since $E(eV) = \frac{hc}{\lambda(nm)\times 1eV}$, h is the Planck constant, 6.63×10^{-34} J.s

c is speed of light, 3.0×10^{17} nms^{-1}

$1eV$ is energy in electron-volt, 1.6×10^{-19} J

$$E(eV) = \frac{6.63\times10^{-34}\ \text{J.s}\times 3.0\times10^{17}\ \text{nms-1}}{\lambda\times 1.6\times10^{-19}\ \text{J}}$$

$$\approx \frac{1240}{\lambda(nm)}$$

The band gap is estimated by extrapolating the linear part of graph of $(\alpha hv)^2$ or $(\alpha hv)^{\frac{1}{2}}$ versus *hv* to $(\alpha hv)^2 = 0$ or $(\alpha hv)^{\frac{1}{2}} = 0$. Where the extrapolated line meets $(\alpha hv)^2 = 0$ or $(\alpha hv)^{\frac{1}{2}} = 0$ is the estimated band gap of the film. This is known as Tauc's approach (Dolgonos *et al*., 2016)

iii). CZTS film band gap Variation

CZTS film has a direct band energy in the range of 1.45 – 1.60 eV (Sheng *et al*., 2014). This band variation is attributed to several factors. These include:

- Film thickness, band gap energy as reported in other researchers results increase with increase in CZTS film thickness. The change in band gap energy with increase in thickness may be due to the change in homogeneity and crystallinity of the films ([b]Shinde *et al*., 2013).
- The ratio of (Cu/(Zn + Sn), band gaps reported by other researchers increase with increase in(Cu/(Zn + Sn) ratio. This is because other phases such $Cu_{2-x}S$ are formed as (Cu/(Zn + Sn) ratio increases (Sheng *et al*., 2014).
- Annealing temperatures, band gap reduce with increase in annealing temperatures. This is because as annealing temperature increases the crystalline nature of CZTS film increases (Pawar *et al*., 2014). Also, as annealing temperature increases there is improvement in CZTS purity since other phases such as Cu_2SnS_3, Cu_3SnS_4 are surpressed (Tiong *et al*., 2014).
- Grain size, Band gaps of nanoparticles is given by equation (3.4) (Tumuluri *et al*., 2014):

$$E_g^{nano} = E_g^{bulk} + \frac{h^2}{2Mr^2} \quad (3.4)$$

Where E_g^{nano}, the energy band gap of the nanoparticles is, E_g^{bulk} is the band gap energy of the bulk material, *M* is the effective mass of the system, *r* is the radius of the nanoparticles and *h* is the Planck constant.

From equation 3.4, it is evident that band gap of nanoparticles decreases with increase in grain size.

iv). **Optical Reflectance**

Reflectance is the percentage measure of the ratio of the intensity of incident light to that of the reflected light. It is measured using a spectrophotometer which is capable of reading the visible range as well as the near infrared and UV. The incident light of known wavelength is directed on to the surface of the object of interest and the intensity of the reflected light is measured (Kittel, 2005). Taking the incident light intensity to be I_0 and the reflected light intensity to be I_R, reflectance is given by

$$R = \frac{I_R}{I_o} \times 100\% \quad (3.4)$$

v). Optical Transmittance

Transmittance is the percentage measure of the ratio of the intensity of incident light to that of the transmitted light. It is also measured using a spectrophotometer Light of known wavelength is directed on the surface of the object of interest and the intensity of the transmitted light measured (Callister, 2007). Taking the incident light intensity to be I_O and the transmitted light intensity to be I_T, transmittance (T) is given by:

$$T = \frac{I_T}{I_0} \times 100\% \quad (3.5)$$

vi). Absorbance

This is the percentage ratio of absorbed light intensity to the incident light. It is calculated from reflectance and transmittance as follows (Callister, 2007):

$$A = 100 - (R + T) \tag{3.6}$$

or

$$A = 1 - (R + T) \tag{3.7}$$

where *R* and *T* are reflectance and transmittance respectively.

3.2 Electrical Characterization of CZTS

This can be done by studying the electrical resistivity of CZTS. Electrical resistivity of CZTS, range from 10^{-3} - 10^{-1} Ω.cm ([b]Shinde *et al.,* 2013). CZTS is a semiconductor and its electrical properties can be measured using two point probe system (spreading resistance analysis) and four point probe system. Emphasis will be on 4-point probe system in this research because of its availability. 4-point probe system is a simple apparatus for measuring resistivity of semiconductor samples. In using the system, current is applied to the sample via the outer probes which induces the measured voltage in the inner probes as illustrated in Figure 3.2. Supposing the distance between the probes is equal then sheet resistivity ρ_s is given by:-

$$\rho_s = \left(\frac{\pi}{\ln 2}\right) R_a = 4.532\ R_a \tag{3.8}$$

R_a is average resistance obtained by reversing the outer terminal probes.

Equation (3.8) only works when the thickness *t*, of the sample is less than half the probe spacing *S*.

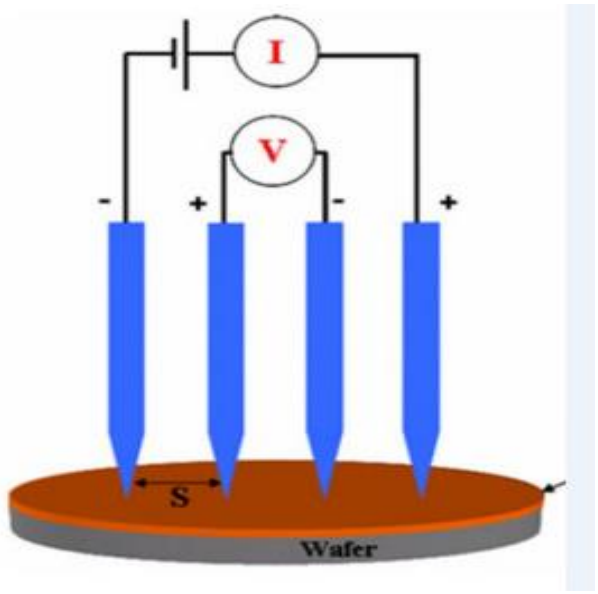

Figure 3.2: Simple set up of 4 point probe system (Smits, 1958).

3.3Defects in CZTS

The defects in CZTS include: amorphous form of film, grain boundary discontinuities, presence of surface states, vacancies ($V_{cu,}$ $V_{Zn,}V_{Sn}$ and V_S), antisite defects ($Cu_{Zn,}$ $Zn_{Cu,}$ Zn_{Sn}, Cu_{Sn}, Sn_{cu} and Sn_{Zn}) and interstitial (Cu_i, Zn_i and Sn_i) defects formed during growth of CZTS (Jiang and Yang, 2013). Antisite defects occur when atoms of different species exchange sites while an interstial defect occurs when an atom occupies a place where no atom would ordinary occupy. Antisite Cu_{Zn} defect is responsible for the observed p-type conductivity of CZTS thin films. This partially explains why CZTS thin film must be Cu-poor and Zn-rich to successfully fabricate CZTS films. These defects increase the resistivity of CZTS, reduces transmittance of CZTS, and acts as an intrinsic doping to the cell making it a p-type semiconductor (Jiang and Yang, 2013).

3.4 Redox Potentials of Cu, Zn and Sn metals

Redox potential consists of reduction and oxidation potential during an electrochemical process. The standard redox potentials of Cu, Zn and Sn metals relative to the standard hydrogen electrode potentials of +0.00 V are 0.52, -0.76 and -0.14 V (Millazo *et al*., 1978).

Since standard reduction potentials in most tables are prepared relative to the standard hydrogen electrode potentials of +0.00 V, and because it is rarely used as a reference electrode, it is necessary to convert an indicator electrode's potential to its value when using a different reference electrode. In this research Ag/AgCl reference electrode has been used. The potential of Ag/AgCl relative to the standard hydrogen electrode is +0.20 V at temperature of 25^{o}C. This potential is added to convert the potential relative to Ag/AgCl reference electrode to that of standard hydrogen electrode, and subtracted to convert from potential relative to standard hydrogen electrode to that of Ag/AgCl reference electrode.

3.5 Determination of Quality of CZTS Film using Raman Spectroscopy

Raman spectroscopy is one of the most powerful tools for determining the crystalline structure and quality of a semiconductor thin films, since the shape and position of Raman peaks are strongly influenced by the presence of defects in a material, either inform of structural inhomogenities or secondary phases (Dimitrievska *et al*., 2014). From Raman spectrum peaks attributed to different compounds in the film is determined by comparing the peaks to already determined theoretical peaks. The Raman spectrum is also important in determining the presence of minor secondary phases in CZTS, which can be related to the Cu-rich and Zn-poor conditions (Liu *et al*., 2010). No other phases exist in quality CZTS after proper heat treatment (Guo *et al*., 2010).

It is necessary to know at what energies occurs the Raman peak for CZTS and other possible phases in CZTS. The Raman peaks at 288 - 289 cm^{-1} and 338 - 339 cm^{-1} are known for quaternary CZTS (Fernandez *et al*., 2011). The strongest peak, 338 - 339 cm^{-1} is attributed the vibration of sulphur atoms (Fernandez *et al*., 2010). Peak appearing at 351 cm^{-1} is related to conditions which are not clear (Lydia and Reddy, 2013). Peaks at 352 and 275 cm^{-1} are attributed to ZnS as one the phases in CZTS (Dimitrievska *et al*., 2014). Tetragonal Cu_2SnS_3 is shown to be present in CZTS by the peaks at 297 cm^{-1}, 337 cm^{-1} and 352 cm^{-1}, this phase can be suppressed by high temperature treatment (Fernandez *et al*., 2011). The cubic Cu_2SnS_3 phase is presented by 267 cm^{-1}, 303 cm^{-1} and 356 cm^{-1} peaks from Raman spectrum. Orthorhombic Cu_3SnS_4 has only one peak at 318 cm^{-1}, SnS has three peaks at 160 cm^{-1}, 190

cm^{-1} and 219 cm^{-1}, SnS_2 has a peak at 314 cm^{-1} and Sn_2S_3 has peaks at 52 cm^{-1}, 60 cm^{-1} and 307 cm^{-1} (Fernandez *et al*., 2011).

CHAPTER FOUR: MATERIALS AND METHODS

4.1 Substrate preparation and cleaning

The chemicals used in this study were of analytical grade and were procured from Alpha Chemica, India.

Conducting glasses (TCO coated glasses) were used as the substrates. The substrates were cleaned by soaking in a mixture of 50 mM of sodium hydroxide and detergent in a beaker for 30 minutes, to etch out dirt on the surface. These substrates were then scrubbed one by one using a piece of cotton wool to complete the removal of dirt. The substrates were then dipped into another beaker containing distilled water and into ultrasonic cleaner for 5 minutes. The substrates were farther ultrasonicated in a beaker containing ethanol for 5 minutes and then rinsed with distilled water. The process was continued using acetone which was also placed into ultrasonic cleaner for five minutes; in order to remove greasy substance from the surface of the substrates. The cleaned substrates were left to dry in a closed area to prevent contamination by dust. Summary of the process is shown in the Figure 4.1:

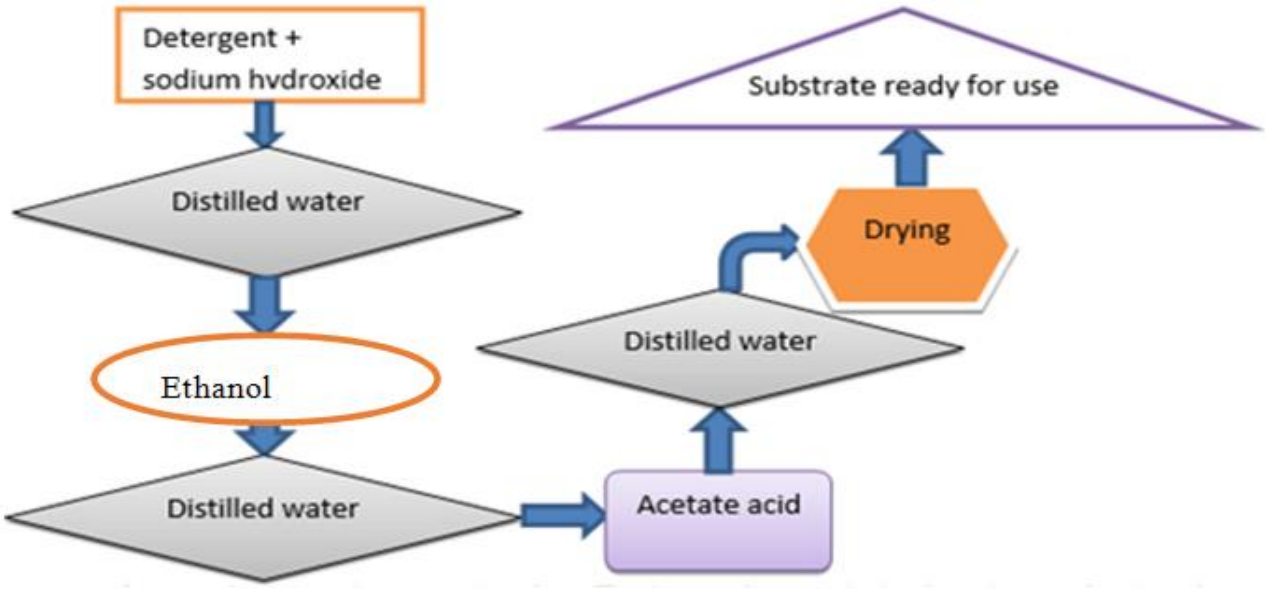

Figure 4.1: Summary of steps during substrate cleaning. Each step is coupled with ultrasonic cleaning with exception of the first and last step.

4.2CZTS Thin Film Deposition

Before the main CZTS thin film deposition individual sulphides of the metals were deposited first, that is, CuS, ZnS and SnS and their optical properties analyzed.

4.2.1 Deposition of CuS Thin Film

CuS was deposited at room temperature (24^{o}C) by electrodeposition coupled with chemical bath method. In electrodeposition 47 mM of $CuSO_4.5H_2O$ was used as a source of copper. The solution was prepared by using distilled water as a solvent. During electrodeposition a potentiostat, Autolab PG STAT 12, Netherlands, was used in the University of Nairobi. An electrochemical cell with three electrodes: RE-Ag|AgCl (saturated KCl), CE-Pt wire and WE- a TCO coated glass was used. Deposition of copper was carried out by linear sweep method with initial potential at -0.10 V and final potential at 0.80 V, since the reduction potential of Cu^{2+} ions was within this range. Several substrates were used and deposition time varied to ensure thickness variation. The formed copper thin film was finally chemically bathed in 50 mM Na_2S solution for 5 minutes to form CuS thin film.

4.2.2 Deposition of ZnS Thin Film

ZnS was synthesized at room temperature by electrodeposition coupled with chemical bath method. In electrodeposition 450 mM of $ZnSO_4.5H_2O$ was used as a source of zinc. The solution was prepared by using distilled water as a solvent. During electrodeposition a potentiostat, Autolab PG STAT 12, was used. An electrochemical cell with three electrode: RE-Ag|AgCl (saturated KCl), CE-Pt wire and WE- a TCO coated glass was used. Deposition was carried out using linear sweep method with initial potential at -1.00 V and final potential at 1.00 V, since the reduction potential of Zn^{2+} ions was in this range. The deposited Zn was then chemically bathed in a 100 mM of thiourea (NH_2CSNH_2) solution for five minutes and thin white substance was formed on the substrate. (NH_2CSNH_2) was used instead of Na_2S solution because in the presence of Na_2S, Zn metal deposited on the substrate was etching off, during chemical bath process.

4.2.3 Deposition of SnS Thin Film

Successive ion layer adsorption and reaction (*SILAR)* technique was used to produce SnS, since during chemical bath in either sodium sulphide solution or thiourea solution Sn metal electrodeposited on the substrate was stripping off.

Tin sulphide was deposited on the TCO coated glass by *SILAR* technique using sodium sulphide and tin chloride as the precursors. Tin (IV) chloride ($SnCl_4.5H_2O$) was used as the tin source and sodium sulphide ($Na_2S.XH_2O$) was used as the sulphur source. Distilled water was used as a solvent at a temperature of 25^oC. 1.2 g of Tin (IV) chloride and 1.7 g of sodium sulphide were used. The glass electrode was dipped into the solutions starting with sodium sulphide followed by distilled water then Tin (IV) chloride and lastly distilled water. A summary of the process is shown in Figure 4.2. This was done repeatedly for 10 cycles. As the process continued formation of brown substance was observed on the glass electrode indicating formation of tin sulphide (SnS) (theoretically colour of Tin sulphide is brown). As the number of cycles increased, the brown color intensified showing that the thickness of SnS on glass electrode increased with increase in number of cycles. The sample was left to dry in a covered place to avoid dust contamination.

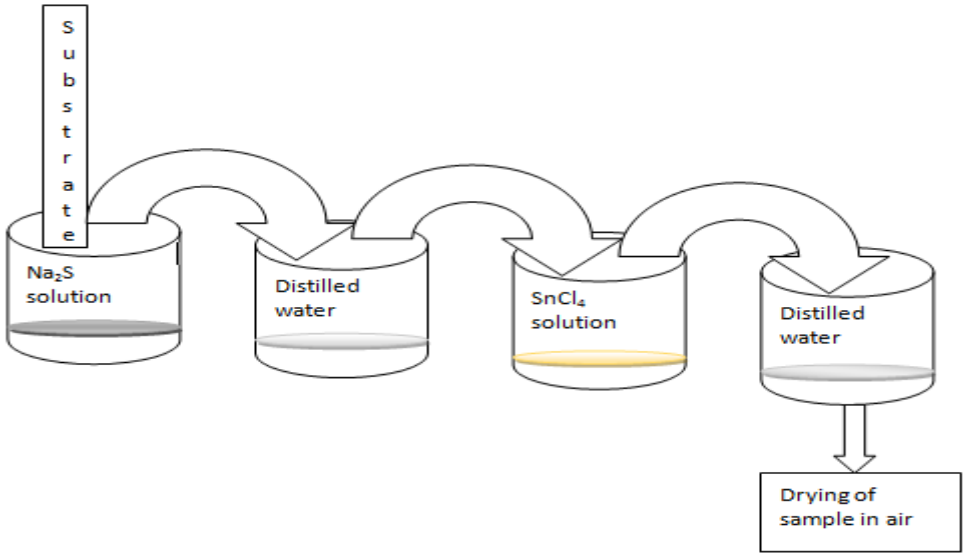

Figure 4.2: Summary of the *SILAR* process.

4.3 Electrodeposition of CZTS

Electrodeposition of CZTS thin films was performed using a three electrode electrochemical cell with a saturated calomel electrode (SCE) as a reference electrode, TCO coated glass as a working electrode and platinum as a counter electrode at room temperature (23^{o}C). Deposition of CZT was done using two methods i.e. layering method and co-electrodeposition method. This was done by the use of Autolab PG STAT 12. Cyclic voltammograme (CV) scan and linear sweep scan were done on the individual solution of zinc sulphate ($ZnSO_4.7H_2O$), tin chloride ($SnCl_4.5H_2O$) and copper sulphate pentahydrate ($CuSO_4.5H_2O$) to determine deposition potentials of the three metals of interest i.e. Cu, Zn and Sn.

4.3.1Preparation of the Solutions

47 mM of $CuSO_4.5H_2O$ was prepared by dissolving $CuSO_4.5H_2O$ in distilled water. This solution was used as a copper source during electrodeposition. 450 mM of $ZnSO_4.7H_2O$ was prepared by dissolving $ZnSO_4.7H_2O$ in distilled water. This solution was used as a source of Zn metal during electrodeposition. 260 mM of $SnCl_4.5H_2O$ was prepared by dissolving $SnCl_4.5H_2O$ in 10 ml of 99.7% acetic acid at a temperature of 90^{o}C then topped up with distilled water to 100 ml was and the resulting solution was used as a source of Sn metal during electrodeposition.

In one step electrodeposition/co-electrodeposition of the three metals, equal volumes (10 mL) of 47 mM $CuSO_4.5H_2O$ and 450 mM $ZnSO_4.7H_2O$ were mixed together, then another 10 mL of 260 mM of $SnCl_4.5H_2O$ was added. The solutions were mixed together but there was formation of suspension which could have been due to formation of $ZnCl_2$. The suspension was cleared by adding 5 ml of 99.7% HCl. This solution never formed suspension and was stable for 7 days indicating its suitability for use.

4.3.2Electrodeposition of CZT Thin Film

The following methods were used in the electrodeposition of CZT thin film:

(i) Layering method

(ii) Co-electrodeposition/one step-electrodeposition method

4.3.3Layering Method

After performing linear sweep on the individual metals it was observed that the electrodeposition direction of Sn was different from that of Zn and Cu, that is, the electrodeposition direction of Sn was the stripping direction for Cu and Zn. Hence electrodeposition was done in layers with Sn being the underneath layer and Cu/Zn composite as the top layer. This layering order was arrived at when it was observed that Sn and Zn were being stripped off the substrate during chemical bath. In attempt to avoid this; layering sequence was decided on.

Sn layer was deposited by performing a linear sweep on 260 mM of $SnCl_4.5H_2O$ solution with the beginning potential of 1.00 V and end potential at -1.00 V, the rate of scan was 0.10 V/s while step potential was 3.05 mV. The deposition was done on a number of substrates using scans of 50, 100 and 150 to get the various Sn thicknesses.

Cu/Zn composite layer was deposited on top of Sn layer by linear sweep in 47 mM of $CuSO_4.5H_2O$ and 450 mM of $ZnSO_4.7H_2O$ solution with the beginning potential of -1.00 V and end potential at 1.00 V. The scan was rate done at a rate of 0.10 V/s and step potential of 3.05 mV was used. The number of scans for each sample was in accordance with the number of scans of Sn. This was to keep Sn, Cu and Zn ratio constant.

4.3.4 Co-electrodeposition Method

According to the study by Septina *et al.,* 2013 the electrolyte consisted of 47 mM of $CuSO_4.5H_2O$, 450mM of $ZnSO_4.7H_2O$ and 260 mM of $SnCl_4.5H_2O$ and two acids (5ml concentrated hydrochloric acid and 10 ml concentrated acetic acid) which were used in formation of homogeneous solution. Co-electrodeposition was performed at a constant voltage of -1.2 V in a multifunction constant voltage mode of the potentiostat. Deposition time was 120 seconds for the different samples deposited. Any deposition time beyond this resulted in film peeling off. The objectives and the parameters of this study were however different from those of Septina *et al.,* 2013.

4.4 Chemical Bath (Deposition of Sulphur on the Deposited CZT) Sulfurization

Sulphurization of the samples was done using chemical bath technique together with annealing step in sulphur rich atmosphere. Chemical bath technique was implemented by dipping and leaving the samples in a 50 mM Na_2S solution for 5 minutes for each sample.

Finally the samples were anealed at various temperatures, 450^{o}C, 500^{o}C and 550^{o}C, in a sulphur rich atmosphere for 30 minutes under the flow of nitrogen gas, using Lab Tech (LEF-4025-3) and then left to cool naturally to avoid film cracking. The annealing temperatures were: 450^{o}C, 500^{o}C and 550^{o}C. Sulfur rich atmosphere was created by evaporating non-harmful organic sulphur powder in a porcelain boat and the vapor directed into the CZTS annealing chamber by the flowing nitrogen gas.

4.5 Elemental Characterization of the CZT Deposited

To determine the elemental composition of the deposited film, Laser Induced Breakdown Spectroscopy (LIBS) (in the University of Nairobi) was used to analyze the deposited CZT film. The scan was done on sampled areas of each film with optical distance from the film of 3 mm, and laser energy of 7.5 mJ. The scans were also done on different areas of a TCO coated glass to get average composition of the film. In using LIBS, a pulsed laser beam is focused onto the sample to be analyzed. Radiation energy is locally coupled into the material and the material starts to evaporate. Within this material vapour and the surrounding gas atmosphere plasma is generated leading to the excitation of the material constituents and spontaneous emission of radiation. The plasma decays and emits elements specific radiation. This emission is resolved spectrally and detected by a spectrometer (Gaudiuso *et al.*, 2010). A block diagram for a typical experimental set-up for LIBS experiments is provided in Figure 4.3.

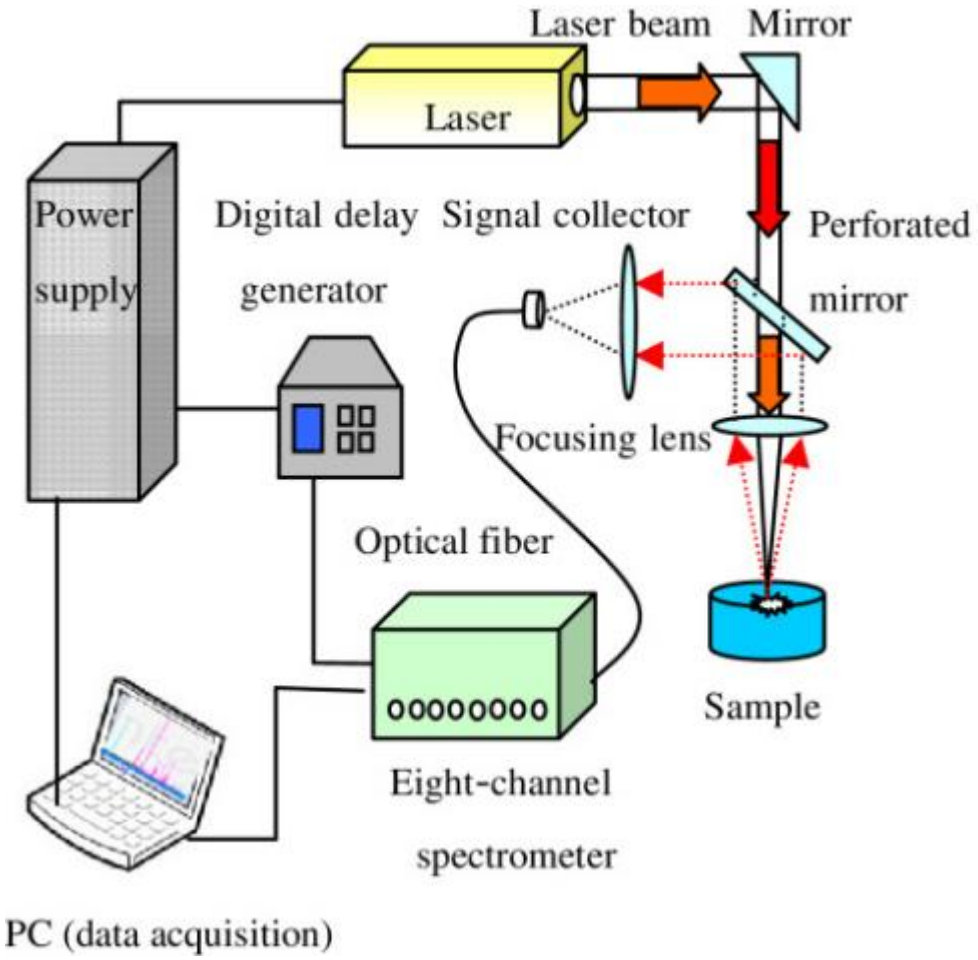

Figure 4.3: A block diagram for a typical experimental set-up for LIBS experiments (Yao *et al*., 2012).

4.6 Quality determination of CZTS Film Formed

Quality determination of CZTS film was done by the use of Raman spectroscopy (in the University of Nairobi) at room temperature at excitation wavelength of 785 nm, exposure time of 10 s, number of accumulation 5 s, center wavelength of 1050 nm, objective ×50 and intensity of 50%. The samples were illuminated with a laser beam in Vis range. Scattered light collected with a lens was sent through spectrophotometer to obtain Raman spectrum of the sample. This was done by randomly sampling different areas on the film. This was then averaged and the spectra of the films drawn as in the results. This was done to identify the crystallinity of the sample as well as other phases present in the resultant films after heat

treatment. Figure 4.4 shows the major components of Raman spectroscopy during operation, which include: laser source, sample illumination system and light collection optics, wavelength selector (filter or spectrophotometer) and detector.

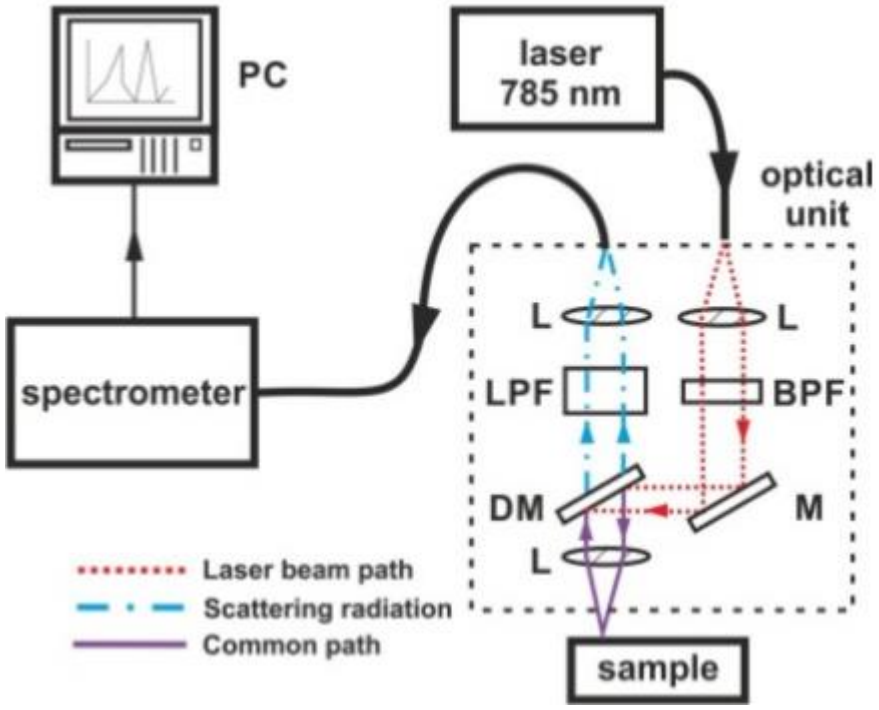

Figure 4.4: A block diagram of major Raman spectroscopy components (Artemyev *et al*., 2014).

4.7Optical and Electrical Characterization

The optical characterization of CZTS was carried out using *Shimadshu UV-VIS-NIR*, Japan spectrophotometer in the wavelength range of 300 – 2500 nm, in the University of Nairobi. The spectrophotometer was a single beam spectrophotometer. Figure 4.5, is a photograph of *Shimadshu UV-VIS-NIR* spectrophotometer in the University of Nairobi.

Figure 4.5: Photograph of *Shimadshu* UV-VIS-NIR spectrophotometer.

4.8 Electrical Characterization

Electrical characterization was done by using four point probe system, Guardian (SRM-232-100), in the University of Nairobi. This done by use of contact technique where a four point probe system was brought into contact with the sample and its sheet resistivity recorded.

CHAPTER FIVE: RESULTS AND DISCUSSIONS

5.1 Cyclic and linear sweep voltammetry

5.1.0 Cyclic Voltammetry (CV) of Copper (Cu)

Cyclic voltammetry was done within a potential range of -1.00 to 1.00 V verses Ag/AgCl. Each cycle started at -1.00 V, reversed at +1.00 V and ended at -1.00 V. A typical CV response of acidified $CuSO_4.5H_2O$ solution is as shown in Figure 5.1. As the scan commenced, the cathodic current density gradually increased until it crossed zero and it turned to anodic current density, and upon reversal of the cycle, the anodic current density gradually decreased until it crossed zero and it turns to cathodic current density. This process repeated itself for the desired number of cycles.

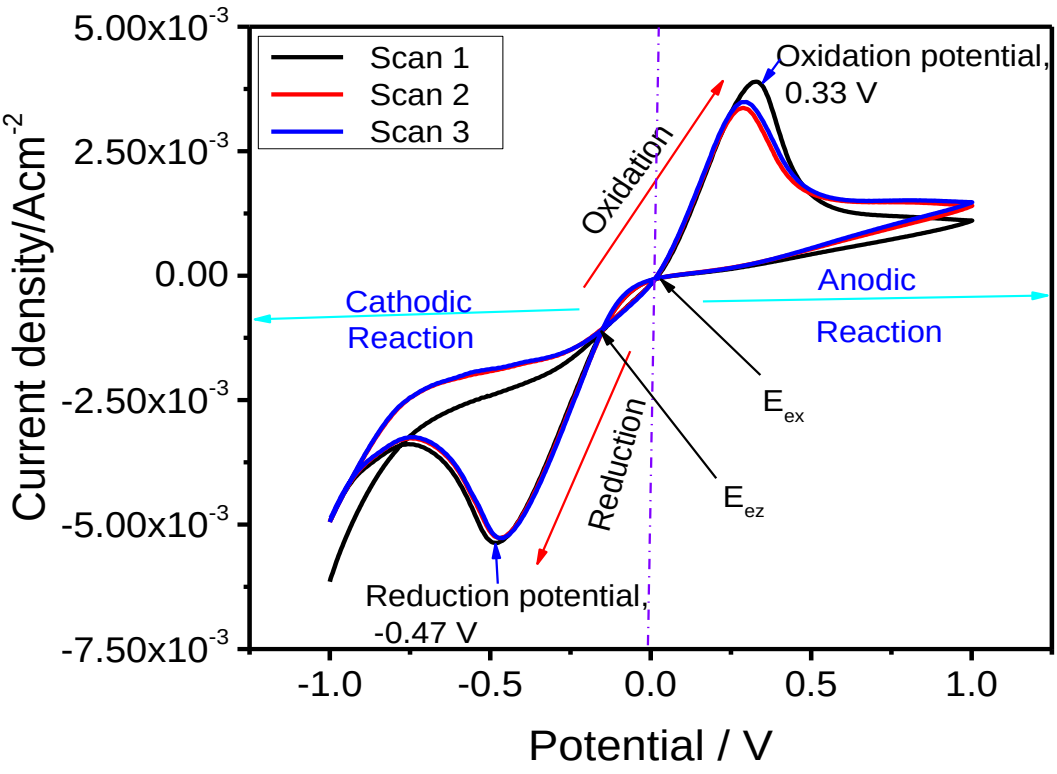

Figure 5.1: CV scans response of Cu electrodeposited on TCO glass electrode in solution containing 47 mM $CuSO_4.5H_2O$. Potential limit -1.00 V to 1.00 V, Scan rate 0.10 V/s, pH 3 and temperature of 23^{o}C.

The solution of $CuSO_4.5H_2O$ used contained Cu^{2+} and SO_4^{2-} ions. The electrochemical process responsible for the reduction peak in the Cu cyclic voltammogram, Figure 5.1, is expressed as:

$$Cu^{2+}_{(aq)} + 2e^- \rightarrow Cu_{(s)} \quad (5.1)$$

The movement of SO_4^{2-} ions in the electrolyte during electrodeposition supports the current flowing in the solution.

The standard redox potential of Cu is ±0.34 V verses Ag/AgCl (Pourbaix, 1974), from the CV scan in Figure5.1, the oxidation peak is observed at +0.33 V verses Ag/AgCl agreeing with result reported by Pourbaix (1974) (Scragg, 2011). In this study reduction potential is observed at -0.47 V verses Ag/AgCl for Cu from the CV scan (Figure5.1). The reduction potential is at a higher negative potential compared to the redox potential of Cu/Cu^{2+}, ±0.34 V. This is in accordance to results reported in other studies (Grujicic and Pesic, 2002).

From the CV scans, the cross over potentials, E_{ex} and E_{ez} are observed at 0.00V and -0.16 V potentials, respectively. These cross over potentials could be due to the difference in deposition and dissolution potentials (Grujicic and Pesic, 2002). In addition, the cross over potential, E_{ez}, could be due to the formation of a new phase involving a nucleation process (Mendoza-Huizar *et al.*, 2009) and E_{ex} could be due to conditional equilibrium potential of couple Cu/Cu^{2+} (Mendoza-Huizar *et al.*, 2009).

5.1.1 Cyclic Voltammetry of Zn

450 mM concentration of $ZnSO_4.7H_2O$ was used as the electrolyte during cyclic voltammetry of Zn. The solution contained Zn^{2+} and SO_4^{2-} ions. The electrochemical process at the WE can be summarized as:

$$Zn^{2+}_{(aq)} + 2e^- \rightarrow Zn_{(s)} \quad (5.2)$$

Figure5.2 shows a typical CV response of acidified $ZnSO_4.5H_2O$. The reduction peak is observed at -0.62 V verses Ag/AgCl and oxidation peak at -0.11 V verses Ag/AgCl. The existence of the oxidation peak in the scan shows that there is presence of Zn electrodeposited during the scan. From theory, Zn is reduced at -0.76 V verses Ag/AgCl (Pourbaix, 1974). The

deviation can be attributed to the conditions at which the experiment was performed, a pH 3 and temperature of 40°C.

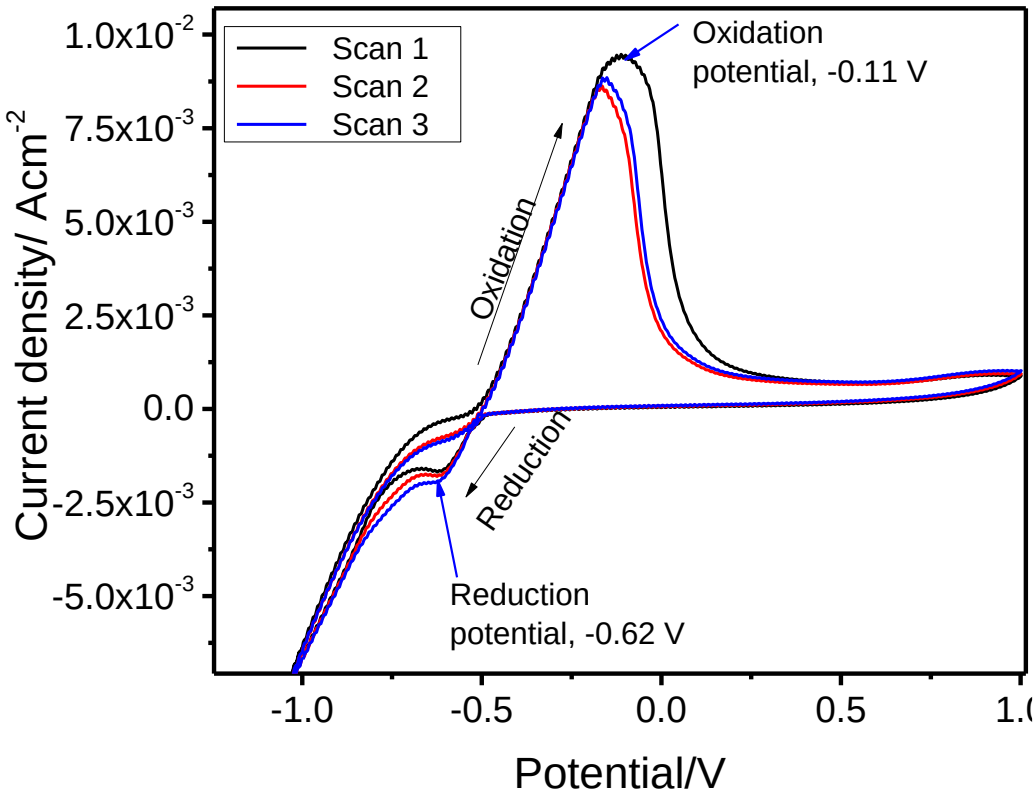

Figure 5.2: CV scans response of Zn electrodeposited on TCO glass electrode in solution containing 450 mM $ZnSO_4.7H_2O$. Potential limit -1.00 V to 1.00 V, Scan rate 0.10 V/s, pH 3 and temperature of 40°C.

5.1.2 Cyclic Voltammetry of Sn

260 mM concentration of $SnCl_4.5H_2O$ was used as the electrolyte during cyclic voltammetry of Sn. The solution contained Sn^{4+} and Cl^- ions. The process at the WE can be expressed as:

$$Sn^{4+}_{(aq)} + 4e^- \rightarrow Sn_{(s)} \qquad (5.3)$$

Cl^- ions ensured flow of current in the electrolyte. Cyclic voltammetry (CV) measurements were performed from -1.00 to 0.00 V versus Ag/AgCl. Figure5.3 shows a typical CV scan of $SnCl_4.5H_2O$. From the data collected the oxidation potential of Sn is -0.33 V verses Ag/AgCl

which is a deviation from the expected -0.13 V verses Ag/AgCl (Scragg, 2011). This shift is due to the presence of acetic acid in the electrolyte, which forms complex ions with tin ions. Reduction peak for Sn from the CV scan is -0.63 V verses Ag/AgCl as indicated in Figure 5.3. The observed reduction peak for Sn is within the theoretical range of reduction peak of Sn which is -0.80 V (Pourbaix, 1974). The presence of one reduction and one oxidation peak shows that reduction process of Sn^{4+} is a single 4-electron step from tin ions to metallic tin.

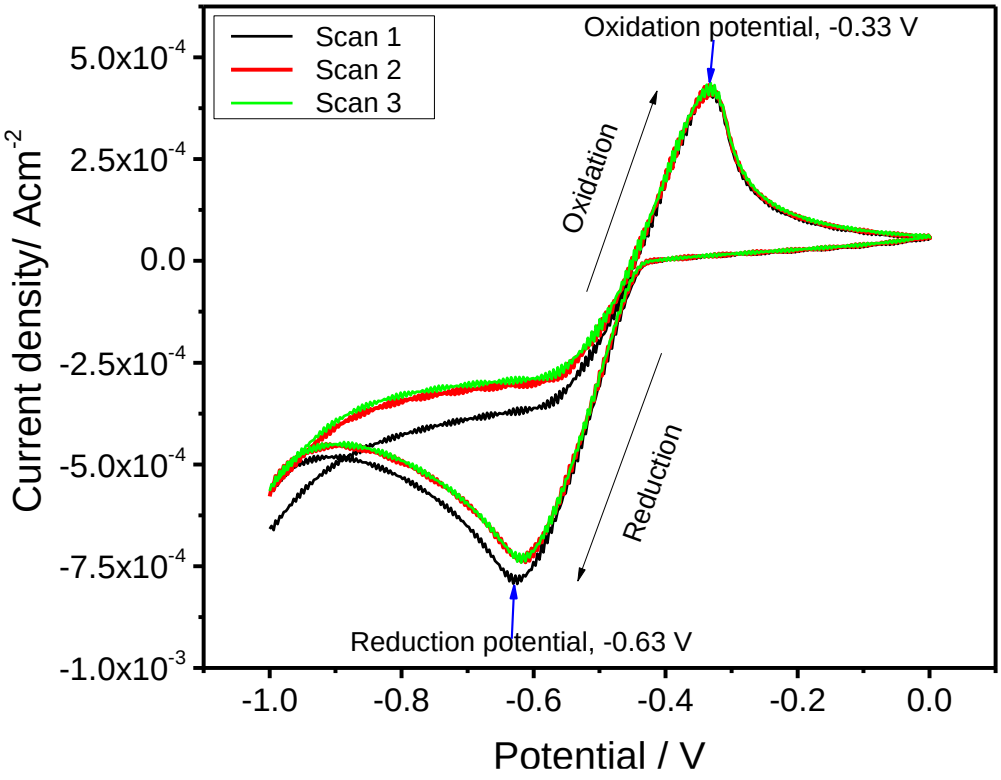

Figure 5.3: CV scans response of Sn electrodeposited on TCO glass electrode in solution containing 260 mM $SnCl_4.5H_2O$. Potential limit -1.00 V to 0.00 V, Scan rate 0.10 V/s, pH 3 and temperature of 23°C.

5.1.3 Cyclic Voltammetry of Zn and Cu

Solution containing 47 mM $CuSO_4.5H_2O$ and 450 mM $ZnSO_4.7H_2O$ was used as the electrolyte during cyclic voltammetry of Cu and Zn. The solution contained Cu^{2+}, Zn^{2+} and SO_4^{2-} ions. The electrodeposition equations are written as:

$$Cu^{2+}_{(aq)} + 2e^- \rightarrow Cu^0_{(s)} \qquad (5.4)$$

$Zn^{2+}_{(aq)}+2e^{-}\rightarrow Zn^{0}_{(s)}$ (5.5)

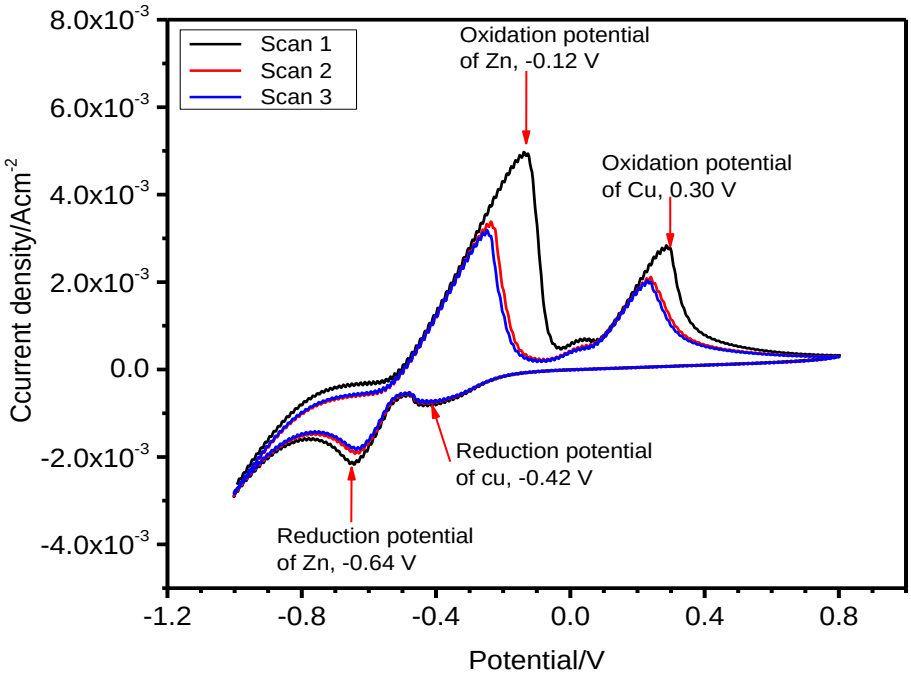

Figure 5.4: CV scans response of Cu and Zn electrodeposited on TCO glass electrode in solution containing a mixture of 47mM $CuSO_4.5H_2O$ and 450mM $ZnSO_4.7H_2O$. Potential limit -1.10 V to 0.80 V, Scan rate 0.10 V/s, pH 3 and temperature of 30^{o}C.

The CV scan performed on electrolyte containing $CuSO_4.5H_2O$ and $ZnSO_4.7H_2O$ showed two oxidation peaks, as shown in Figure 5.4. The oxidation peaks, at -0.12 V verses Ag/AgCl and 0.30 V verses Ag/AgCl, are the oxidation peaks of Zn and Cu, respectively. This result was comparable to the oxidation peaks of individual metals, section 5.1.1 and 5.1.2. The reduction potentials, -0.64 V verses Ag/AgCl and 0.42 V verses Ag/AgCl, were also comparable to the experimental reduction peaks of the individual metals, section 5.1.1 and 5.1.2. This result showed that Zn and Cu could be deposited simultaneously within a predetermined potential range.

5.1.4 Cyclic Voltammetry of Cu, Zn and Sn

Solution containing 47 mM $CuSO_4.5H_2O$, 450 mM $ZnSO_4.7H_2O$ and 260 mM $SnCl_4.5H_2O$ was used as the electrolyte during cyclic voltammetry of Cu, Zn and Sn. The solution contained Cu^{2+}, Zn^{2+} and Sn^{4+} ions. The electrochemical process at the WE (the Cathode), reduction can be written as:

$$Cu^{2+}_{(aq)}+2e^{-}\rightarrow Cu_{(s)} \quad (5.6)$$

$$Zn^{2+}_{(aq)}+2e^{-}\rightarrow Zn_{(s)} \quad (5.7)$$

$$Sn^{4+}_{(aq)}+4e^{-}\rightarrow Sn_{(s)} \quad (5.8)$$

A typical cyclic voltammogram of the three metals is as shown in Figure 5.5: The CV response showed that the three metals can be deposited simultaneously. There is a slight shift in peaks due to ion interactions in the electrolyte.

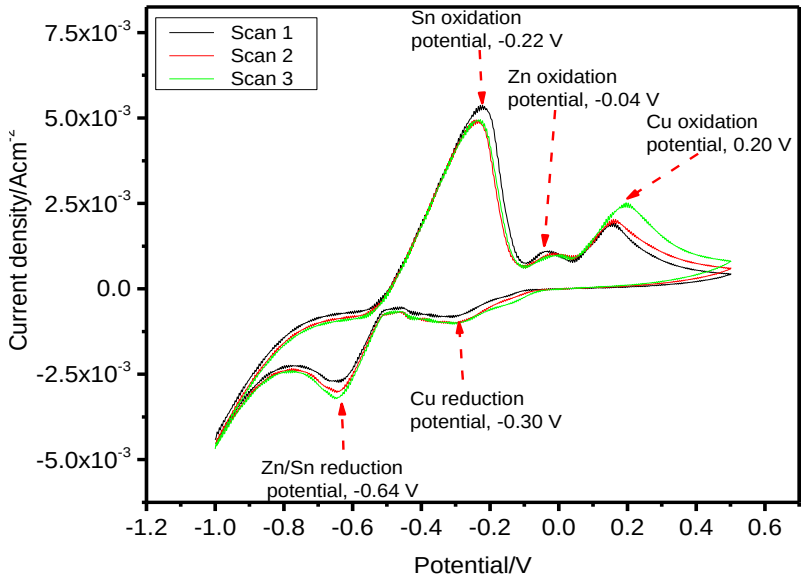

Figure 5.5: CV scans response of Cu, Sn and Zn electrodeposited on TCO glass electrode in solution containing 47 mM $CuSO_4.5H_2O$, 260mM $SnCl_4.5H_2O$ and 450mM $ZnSO_4.7H_2O$. Potential limit -1.00 V to 0.50 V, Scan rate 0.10 V/s, pH 3 and temperature of 27°C.

5.1.6 Linear sweep voltammetry of Sn

Figure 5.6 gives a typical result of linear sweep on $SnCl_4.5H_2O$.

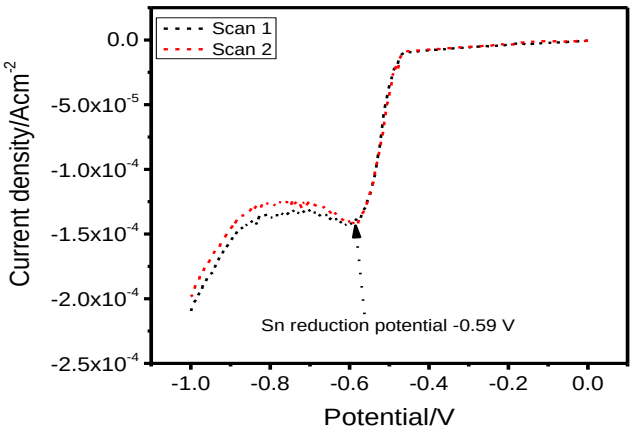

Figure 5.6: Linear sweep scans response of Sn electrodeposited on TCO glass electrode in solution containing 260 mM $SnCl_4.5H_2O$. Potential limit 0.00 V to -1.00 V, Scan rate 0.10 V/s, pH 3 and temperature of 23°C.

The scan shows that Sn is reduced at -0.59 V verses Ag/AgCl for the electrolyte condition used. This result is in line within the range obtained from CV scan which was -0.63 V verses Ag/AgCl. This result showed that Sn could be deposited by linear sweep voltammetry.

5.1.7 Linear sweep voltammetry of Cu and Zn

This method showed that the oxidation potential of Zn is -0.58 V verses Ag/AgCl, and that of Cu is 0.31 V verses Ag/AgCl. The peak heights increased with increase in number of scans showing that conductivity of the substrate increased as deposition takes place. The linear sweep performed on the two metals confirmed the oxidation potential obtained from CV scan of the two metals. Result of linear sweep on Cu and Zn is shown in Figure 5.7.

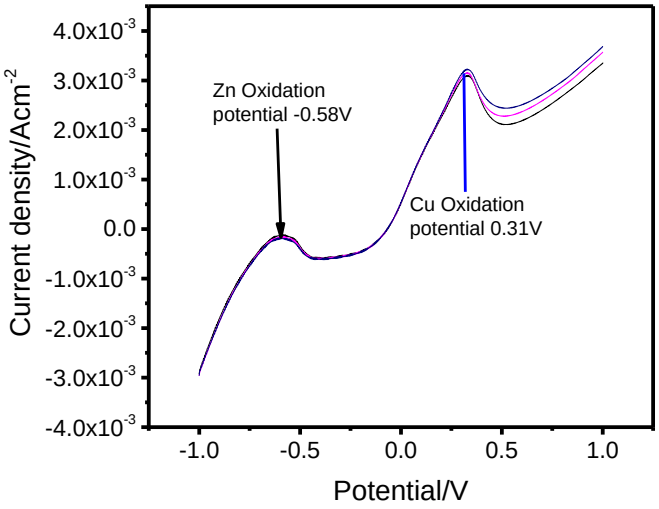

Figure 5.7: Linear sweep scans response of Cu and Zn electrodeposited on TCO glass electrode in solution containing a mixture of 47 mM $CuSO_4.5H_2O$ and 450 mM $ZnSO_4.7H_2O$. Potential limit -1.10 V to 0.80 V, Scan rate 0.10 V/s, pH 3 and temperature of 30^oC.

5.2 Co-electrodeposition of CZT

Co-electrodeposition was done using 47 mM $CuSO_4.5H_2O$, 260 mM $SnCl_4.5H_2O$ and 450 mM $ZnSO_4.7H_2O$. Deposition was done by use of multifunction constant voltage (potentiostat/galvanostat) at a constant potential of -1.20 V verses Ag/AgCl (Araki *et al.*,

2009). The current-time variation graphs for electrodeposition CZT is as shown in the Figure 5.8.

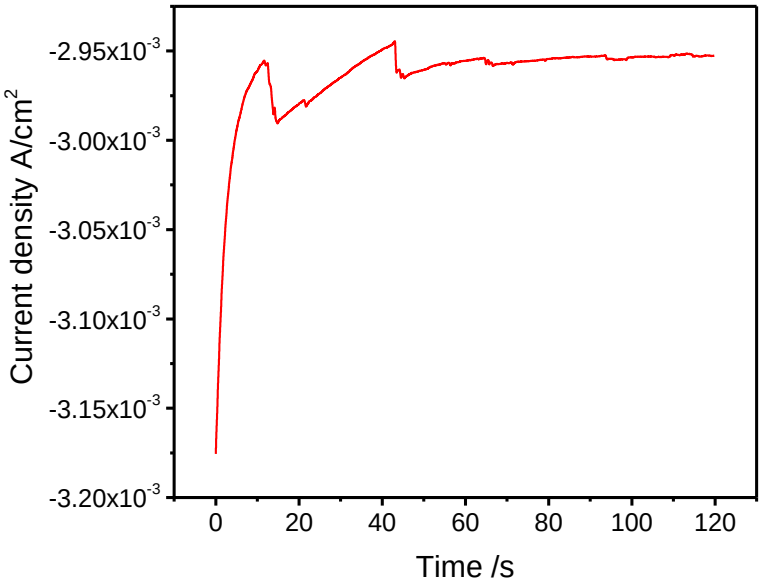

Figure 5.8: Current verses time for the co-electrodeposition of CZT at constant deposition potential of -1.20 V at room temperature. 47 mM of $CuSO_4.5H_2O$, 260 mM $SnCl_4.5H_2O$, 450 mM $ZnSO_4.7H_2O$, pH 3 and temperature 0f 30^oC.

It was observed that, at time zero seconds the current was -3.20×10^{-3} A/cm^2, however as the deposition started the current increased steadily to -2.95×10^{-3} A/cm^2, which the end current. This increase in current is a typical evidence of surface nucleation.

5.3 Elemental Analysis of the Deposited CZT

Elemental analysis of the deposited CZT thin film was done by Laser induced breakdown spectroscopy (LIBS). In determination of the exact elements in the deposited thin layer, an elemental characteration was first done on the TCO glass itself which showed Cu, Zn and Sn as per spectral lines in Figure 5.9.

Elemental characterization of the deposited CZT film was carried out and the spectral lines are as shown in Figure 5.10. However, it was not clear whether the deposit contained the desired elements since the substrate also had the same elements. Therefore to confirm the elements

presentin the deposited thin film, the spectrum of the glass was substracted from that of the glass and the deposit and the result is as shown in Figure 5.11. Figure 5.11 did not show the presence of any sulphur as expected since upto this point no sulphur element had been deposited. Hence, this confirmed the deposition of CZT film.

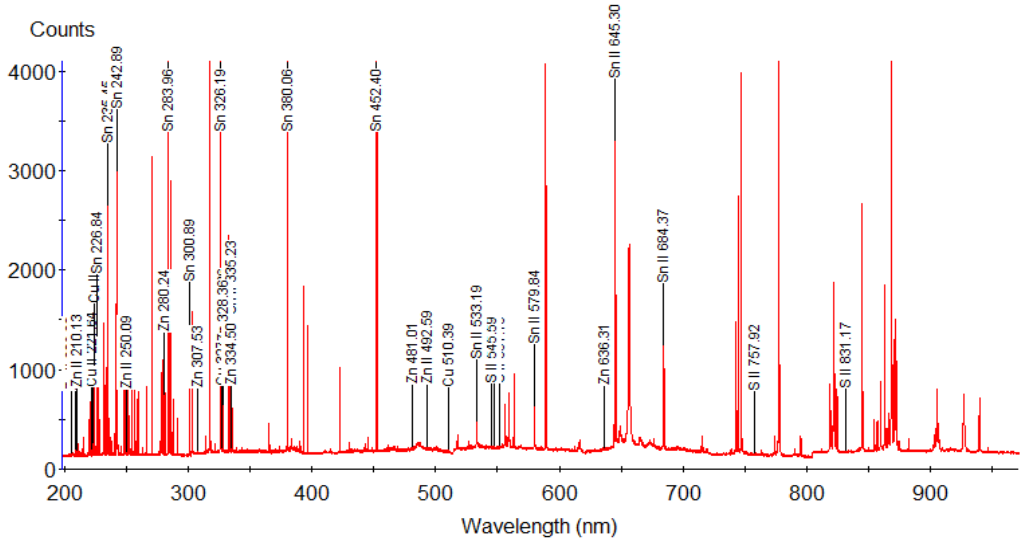

Figure 5.9: Spectral lines of TCO coated glass. Energy 7.5 mJ, integration time 0.42 µS, shot counts 1, single count, Q switch delay time 150 µS and optical distance 3 mm.

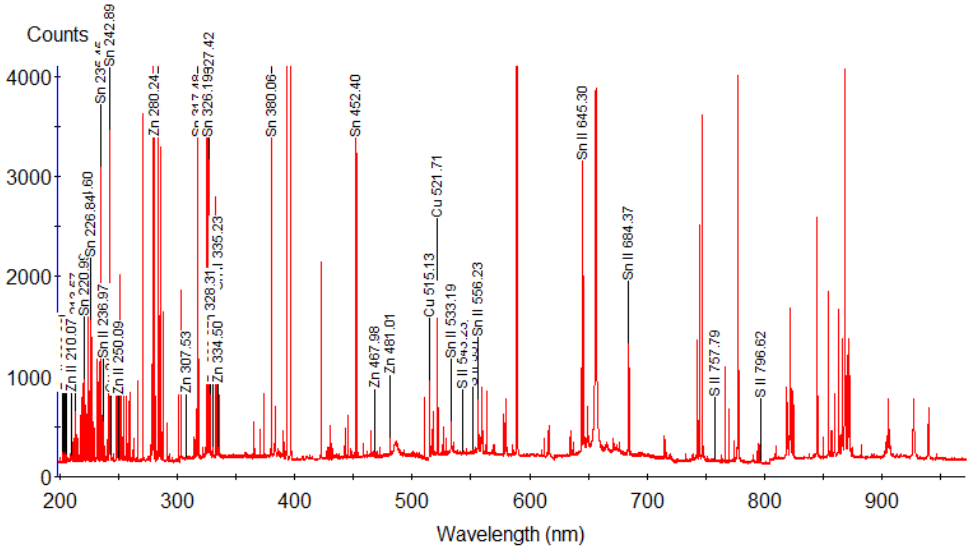

Figure 5.10: Spectral lines of both the deposited CZT film and TCO coated glass. Energy 7.5mJ, integration time 0.42 µS, shot counts 1, single count, Q switch delay time 150 µS and optical distance 3 mm.

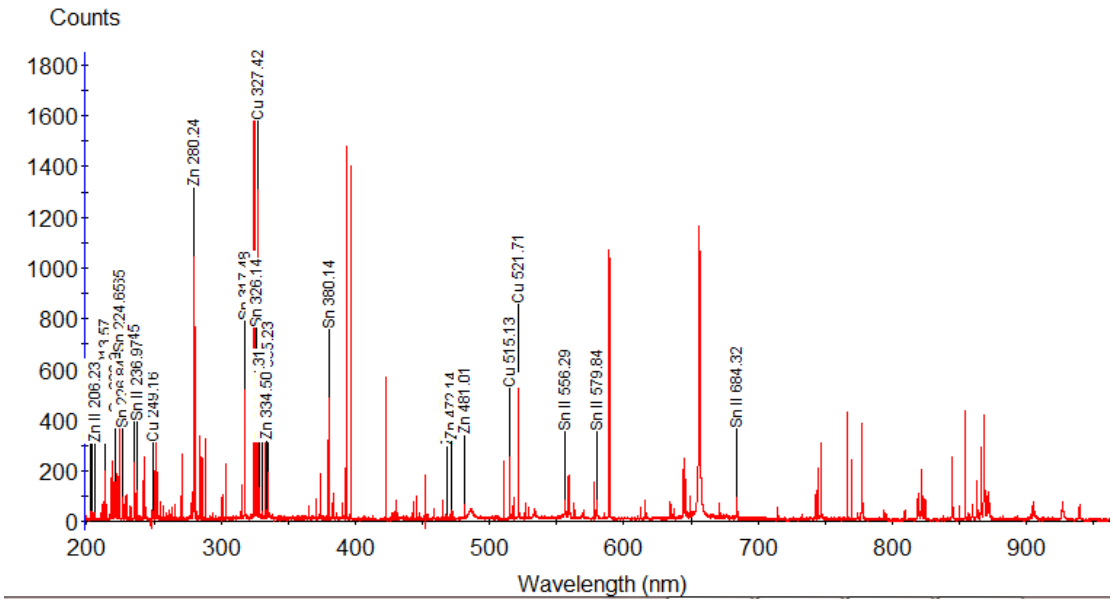

Figure 5.11: Spectral lines of deposited CZT film using LIBS spectroscopy. Energy 7.5 mJ, integration time 0.42 µS, shot counts 1, single count, Q switch delay time 150 µS and optical distance 3 mm.

5.4 CuS Thin Film

5.4.1 Optical Properties of CuS Deposited by Electrodeposition Coupled with Chemical Bath Deposition

A red-brown substance of uniform thickness was observed on the substrate after electrodeposition of Cu metal. Then, CuS was formed by chemical bath deposition as described in section 4.4.

5.4.2 Reflectance and Transmittance of CuS

Reflectance and transmittance curves of CuS obtained using Shimadshu UV-VIS-NIR, Japan spectrophotometer were as shown in Figure 5.12, in the wavelength range of 250 – 2500 nm.

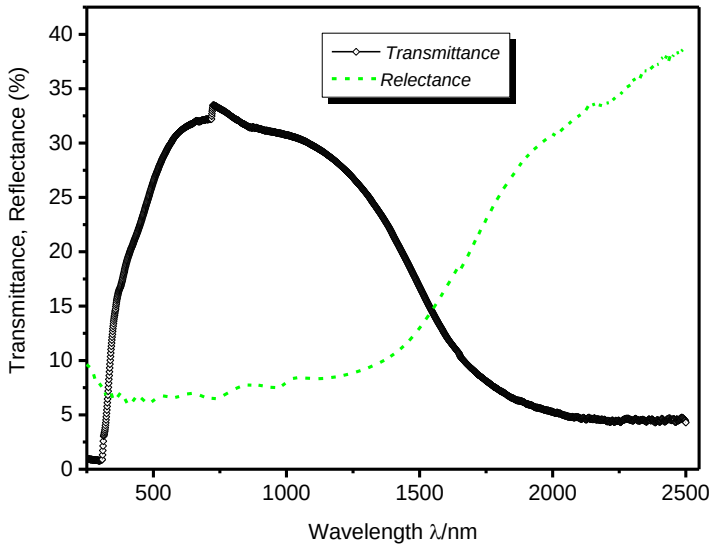

Figure 5.12: Transmittance and Reflectance curves of CuS.

Transmission range was divided into three major regions namely transparent, weakly and highly transmitting regions.

The UV-VIS-NIR transmittance spectrum in Figure 5.12 showed that transmittance of CuS varied with wavelength, and that the transmittances increased from UV (200 – 400 nm) region to visible region (400 – 800 nm) while it decreased at the NIR (900 – 3000 nm). Above 800 nm transmission of CuS film on glass coated with TCO (transparent conducting oxide) decreased with increase in wavelength which is due to high reflectance in this region. From literature, transmittance of CuS in the wavelength region ≤525 nm should be zero due to high absorption in this region (Xie *et al.*, 2014) since band gap of CuS is 2.37eV (Dhasade *et al.*, 2015). According to the result in Figure 5.12 this was not the case which could be due to the small thickness of the deposited film. For long wavelength region, however, there are no appropriate electronic transitions possible hence transmission was expected to be very high. This was not the case according to Figure 5.12. This difference could be attributed to TCO coating on the substrate used (Freeda *et al.*, 2011).

The reflectance spectrum of CuS deposit was also analyzed. For CuS reflectance was low in the region between 200 - 1154 nm. This is because of high transmittance in this region. In the

long wavelength region starting from 1222 nm, reflectance increased due to the effect of TCO coating on the substrate that was used (Cheng *et al.*, 2012).

5.4.3 Band Gap of CuS

From optical transmittance and reflectance data of the film which was measured in the wavelength range of 200 - 2500 nm, absorption coefficient (α) was calculated. From absorption coefficient (α), a graph of $(\alpha h\nu)^2$ against energy $(h\nu)$ was plotted for different film thicknesses.

Absorption coefficient (α) was calculated as (Rahmani *et al.*, 2009);

$$\alpha = -\frac{1}{d}\ln\left(\frac{R_{normalized}}{1-T_{normalized}}\right) \tag{5.9}$$

where *d, R, and T* are defined in section 3.1.

Energy, *E (eV)* is expressed as,

$$E(eV) = \frac{1240}{\lambda(nm)} \tag{5.10}$$

where λ (nm) is wavelength. The graphs were as shown in Figure 5.14.

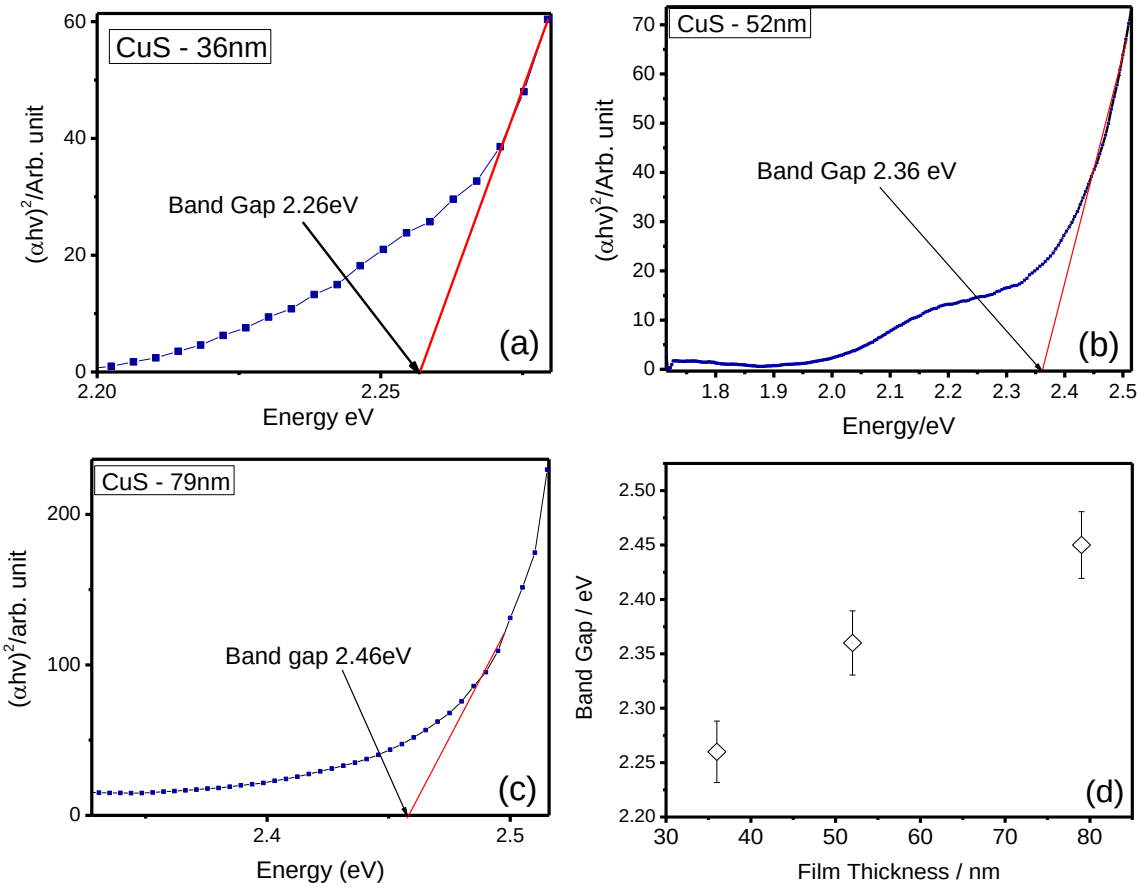

Figure 5.13: Band gap of CuS film (a) 36 nm, (b) 52 nm, (c) 79 nm, and (d). Variation of band gap with thickness for copper thin films

From the work of Dhasade *et al*, 2015 the band gap of CuS is 2.37 eV while from this study the band gap of CuS of 52.00 nm thickness was found to be 2.36 eV while that of 79.00 nm was 2.45 eV. This study showed that band gap varied with thickness, with the best band gap being observed at film thickness of a lower value. Figure 5.13(d) shows that band gap is directly proportional to thickness.

5.4.4 Quality Determination of CuS using Raman Spectroscopy

A Raman spectrum of deposited CuS is presented in Figure 5.14 below. A broad peak due to CuS film was recorded at 469 cm^{-1} and another at 478 cm^{-1} which could be because of the presence of $Cu_{2-x}S$ which normally appears at 475 cm^{-1} (Tiong *et al.*, 2014). The presence of $Cu_{2-x}S$ partly explains the small shifts in CuS band gaps obtained (Figure 5.13, section 5.4.3). This is because $Cu_{2-x}S$ supports the presence of point defects in the CuS film (Shin *et al.*, 2011).

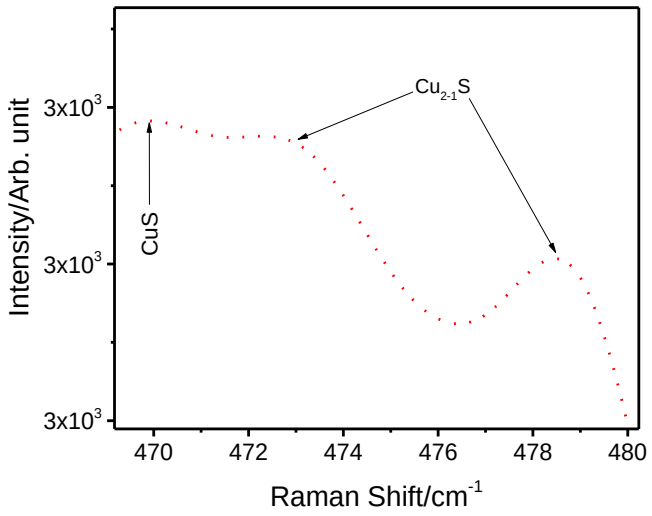

Figure 5.14: Peaks of deposited CuS film. Laser 785 nm, exposure time 10 s, number of accumulations 5 s, objective ×50 and intensity 50%.

5.5 Optical Properties of ZnS Deposited by Electrodeposition Coupled with Chemical Bath Deposition

5.5.1 Reflectance and Transmittance of ZnS

Reflectance and transmittance of spectrum of ZnS from spectrophotometer were as shown in Figure 5.15.

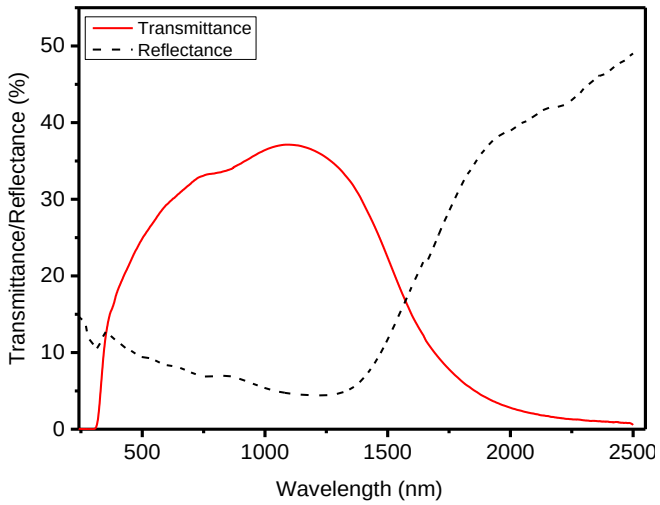

Figure 5.15: Transmittance and reflectance graphs of ZnS.

The UV-VIS-NIR transmittance spectrum in Figure 5.15 showed that ZnS had varying transmittance, and the transmittance was significantly higher in the visible region (400 - 750 nm), the transmittance then decreased at the NIR (750 - 3000 nm) region. Explanation is provided in section 5.4.2.

It was observed that ZnS reflectance was low in the wavelength range of 200 - 1154 nm and this was because of high transmittance in this region. In the long wavelength region starting from 1222 nm, reflectance increased due to decrease in transmission in this region. This increase could also be attributed to TCO coating on the glass as has been explained in section 5.4.2.

5.5.2 Band Gap of Deposited ZnS

The band gap of the as-deposited ZnS was approximated, Figure 5.16.

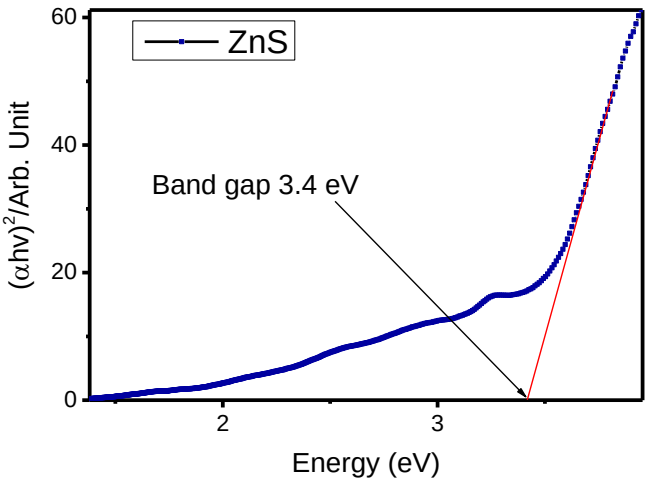

Figure 5.16: Band gap of deposited ZnS thin film.

This study showed that the band gap of ZnS is 3.54 eV which compared very well with the value reported earlier by Borah and Sarma (2008), who showed a band gap of 3.68 eV. These values were within ±3.80% range which is within permissible experimental measurements error. The difference could be due to defects in the deposited thin film e.g. cracks in the film (Borah *et al.*, 2008).

5.5.3 Quality Determination of ZnS using Raman Spectroscopy

The structure of deposited ZnS is presented in Figure5.17.

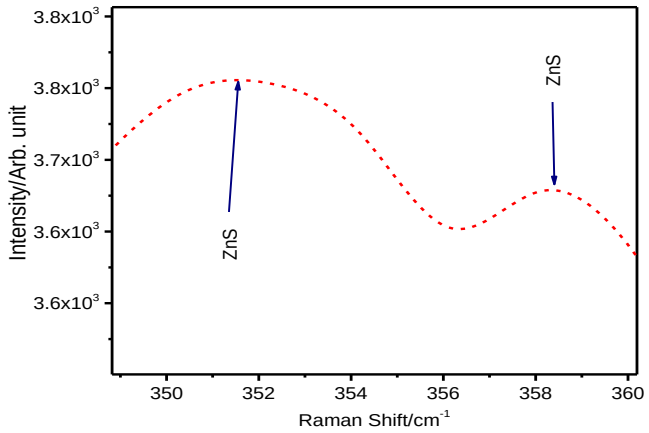

Figure 5.17: Raman shifts of the deposited ZnS. Laser 785 nm, exposure time 10 s, number of accumulations 5 s, objective ×50 and intensity 50%.

A sharp peak was observed at 358 cm^{-1} and a wide peak at 350 cm^{-1}; which are the main peaks of ZnS (Tiong *et al.*, 2014). The shifts in the peaks could be due to non-uniformity of the film thickness. This structural characterization clearly confirmed that ZnS was deposited on the TCO coated substrate.

5.6 Optical Properties of SnS Deposited by *SILAR* Method

5.6.1 Reflectance and Transmittance of SnS

Reflectance and transmittance of ZnS from spectrophotometer were as shown in Figure 5.18.

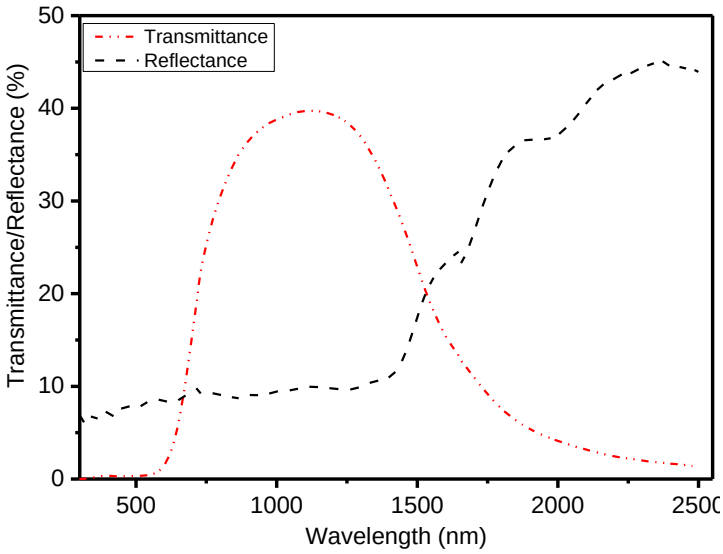

Figure 5.18: Transmittance and reflectance of SnS deposited by *SILAR* technique.

The transmission range divided into three major regions transparent, weakly and highly transmitting regions. In the region ≤500 nm, there was no transmission due to high absorption of SnS in this region, in addition, the radiations in this region were either cut or absorbed by TCO coating on the glass. Above 800 nm transmission of SnS film was decreasing with increase in wavelength due to increasing reflectance (Figure 5.18). According to Cheng *et al.*, 2012, the transmission of SnS coated on a plane glass increased with increase in wavelength in the long wavelength region. Therefore this decrease in Transmission of SnS in long wavelength region can be attributed to the TCO coating of the glass.

For SnS reflectance is very low and appears to be decreasing in the wavelength range of 330 - 1230 nm according to the graph above this is because of increase of transmission in this region. From 1230 nm reflectance increases, which is exactly opposite of what should be the result (Cheng *et al.*, 2012).This could be attributed to the TCO coating on the glass.

5.6.2 Band Gap of SnS

Figure 5.19 shows the direct and indirect band gaps of the as-deposited SnS thin film.

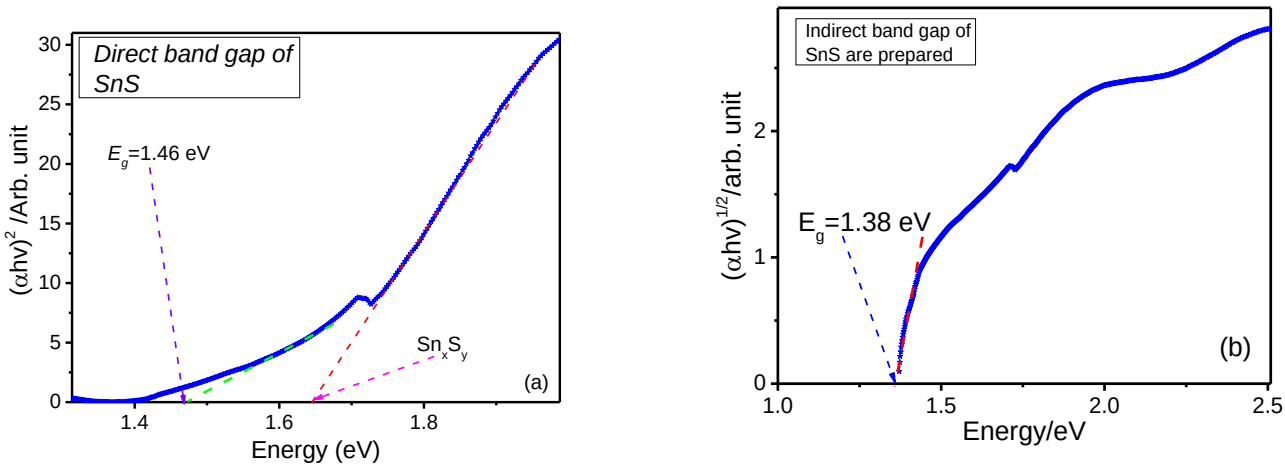

Figure 5.19: (a) Direct,(b) indirect band gaps of as-deposited SnS.

The direct band gap of SnS from the study was 1.46 eV which is within range of standard value of 1.3 - 1.5 eV (Umar *et al.*, 2013). The indirect band gap of SnS from the experiment is 1.38eV lying out of range of the standard value which is 1.0 - 1.1 eV (Umar *et al.*, 2013). SnS_2 and Sn_2S_3 and poor crystallinity of the films may have lead to higher optical band gap (Hegde *et al.*, 2011). In addition this result was obtained before annealing and there could be presence of minute water molecules in the sample.

5.7 Optical Properties of CZTS Deposited by Electrodeposition Coupled with Chemical Bath Technique

5.7.1 Optical Properties of As-Deposited CZTS Deposited by Layering Method

Reflectance and transmittance of as-deposited CZTS from spectrophotometer are presented in Figure 5.20. The measurement was done on samples prepared under different conditions.

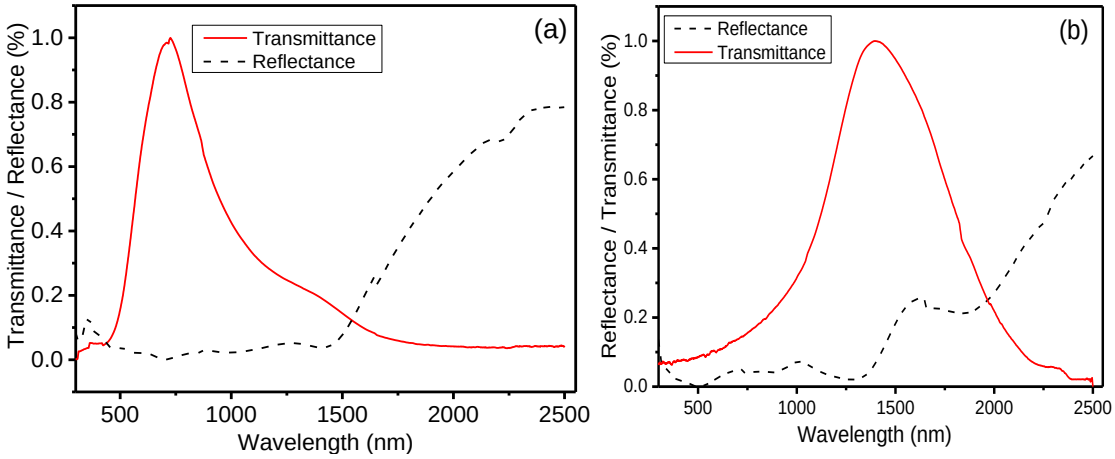

Figure 5.20: Transmittance and reflectance of as-deposited CZTS deposited by layering method followed by chemical bath in Na_2S solution.(a) 130 nm, and (b) 250nm

The UV-VIS-NIR transmittance spectrum showed that the transmittance of CZTS increased within wavelength range of 400 - 700 nm then decreased gradually thereafter. From the transmittance curve of CZTS thin film deposited it was observed that the transmittance of as-deposited CZTS was low in the visible region with a percentage transmittance of 21 - 25%. The low reflectance of CZTS (Figure 5.20) observed in the visible region could be due to high absorbance and transmittance in this region.

5.7.1.1 Band Gap of As-Prepared CZTS by Layering Method

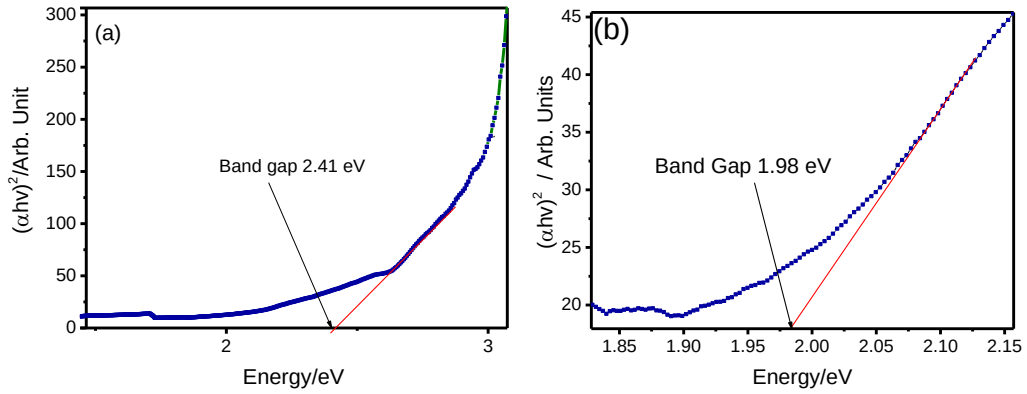

Figure 5.21: Band gap of as-deposited CZTS deposited by layering method followed by chemical bath in Na_2S solution. (a) band gap of 250 nm and (b) band gap of 130 nm CZTS.

The plot of $(\alpha hv)^2$ versus (hv) was found to be linear. The band gap of as-deposited CZTS in this study ranged between 1.98 eV to 2.41 eV, Figure 5.21. The band gap changed with deposition time implying that band gap is a function of thickness. The band gap was high since in the as-deposited status was amorphous in nature. The high band gap could be due to solid solutions and other phases ([a]Shinde *et al.*, 2013). The change in band gap with film thickness may be due to change in homogeinity and crystallinity of the films (Pawar *et al.*, 2014). The change in thickness is as a result of change in particle sizes resulting in change in band gap (Lydia and Reddy, 2013).

5.7.1.2Optical Properties of Annealed CZTS Thin Film prepared by layering Method

Reflectance and transmittance of annealed CZTS, prepared by layering method, at 450^{o}C from spectrophotometer were as shown in Figure 5.22.

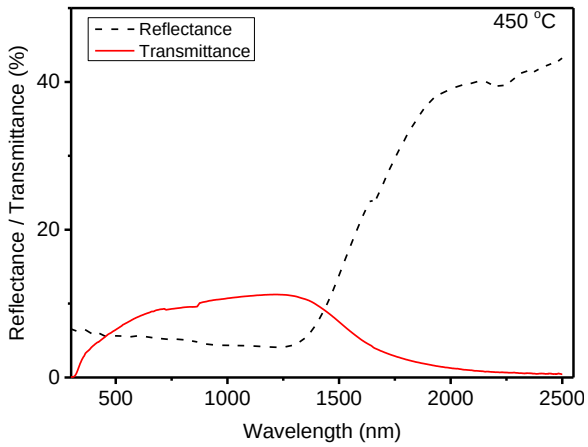

Figure 5.22: Transmittance and reflectance of CZTS deposited by layering method followed by chemical bath in Na_2S solution annealed at 450°C.

The transmittance of CZTS annealed at 450°C as shown in the Figure 5.22 increased in the visible region i.e. 319 - 668 nm, to attain a percentage transmission of 9.1%. In the wavelength range of 871 - 1213 nm transmittance was observed to increase until it attained a higher percentage of 11%. Reflectance for the sample above is very low at 4%

Reflectance and transmittance of annealed CZTS, prepared by layering method, at 500°C is presented in Figure 5.23.

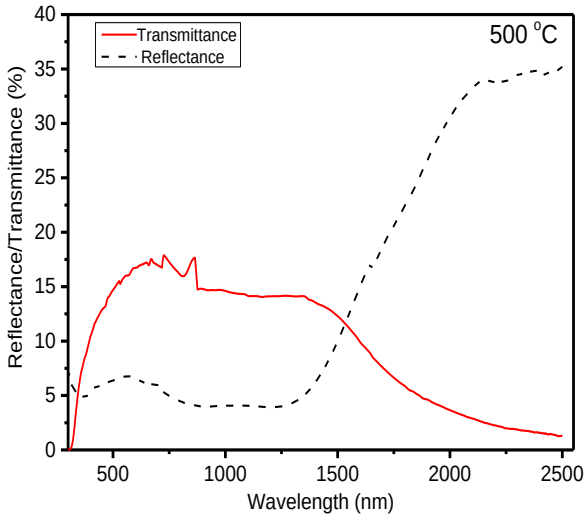

Figure 5.23: Transmittance and reflectance of CZTS deposited by layering method followed by chemical bath in Na_2S solution annealed at 500°C.

The transmittance of CZTS annealed at 500°C is shown in Figure 5.23, indicated that transmittance increased in the visible range region i.e. 335 – 620 nm, to attain a percentage transmission of 17% in this region. The two spikes shown on the transmittance could be due to change of detector of the spectrometer. At wavelength of 880 nm, transmittance was observed to decrease. Reflectance in Figure 5.23 was very low at 4%.

Reflectance and transmittance of annealed CZTS, prepared by layering method, at 550°C is as shown in Figure 5.24.

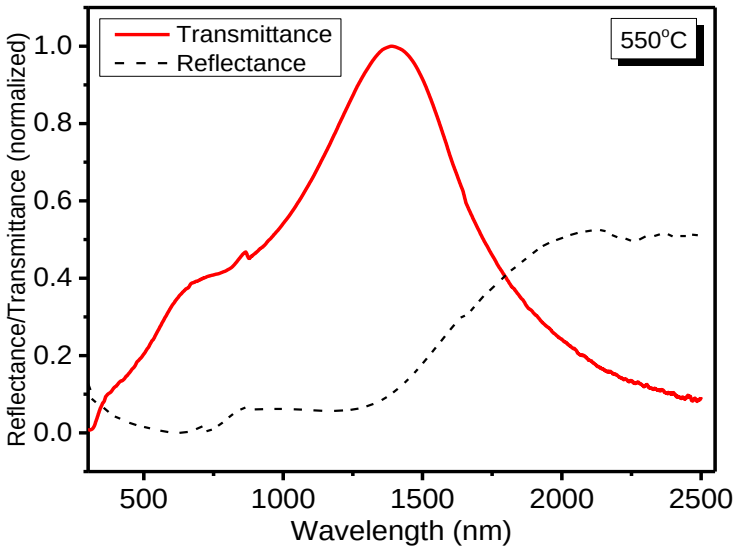

Figure 5.24: Transmittance and reflectance of CZTS deposited by layering method followed by chemical bath in Na_2S solution annealed at 550°C

The transmittance of CZTS annealed at 550°C as shown in the Figure 5.24 increased in the visible range region i.e. 327 – 676 nm, to attain a percentage transmission of 2.7% in this region. The study showed that transmittance tends to increase with wavelength in the long wavelength region i.e. 880 - 1368 nm, to attain a percentage transmission of 6.6%. However, transmittance is finally observed to decrease with wavelength, an observation that was not expected but this could be attributed to the TCO coating on the glass used.

The results further showed that the transmittance of CZTS annealed at 550°C was low which implied that the absorbance of the deposited thin film was high across the whole solar spectrum range. This property was observed to be best for photovoltaic application since absorption is not only able to occur in the highly appreciated visible region but in the whole solar spectrum.

The reflectance of CZTS annealed at 550°C as shown in Figure 5.25 was very low, 4% which implied that maximum light reached the surface of the sample. Applying the relationship, $A+R+T=100\%$ (where A, R and T are absorbance, reflectance and transmittance respectively) it was observed from the transmittance and reflectance data of CZTS annealed at 550°C that absorbance (A) was high for this material.

Generally transmittance should decrease with increase in annealing temperature up to the optimum temperature which according to this study is 550^{o}C. However, this study did not clearly show this variation in transmittance with temperature according to transmittance graphs of CZTS obtained.

5.7.1.3 Band Gap of CZTS after Annealing Thin Film Prepared by Layering Method

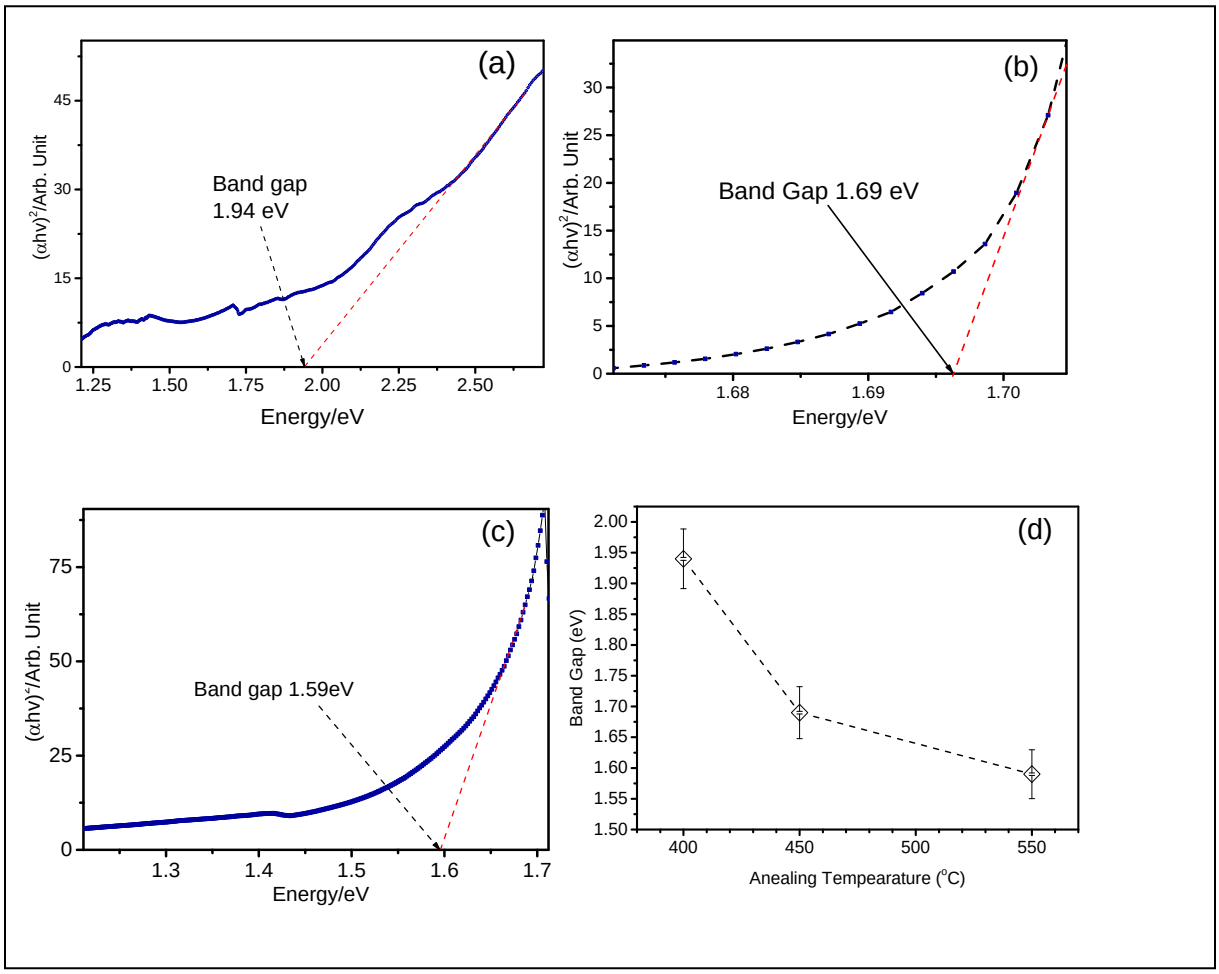

Figure 5.25: Band gap of CZTS deposited by layering method followed by chemical bath in Na_2S solution and annealed at: (a). 450^{o}C, (b) 500^{o}C (c) 550^{o}C and (d) the variation of band gap with annealing temperature.

The band gap of CZTS after annealing under nitrogen gas flow at 450^{o}C in sulphur vapor was found to be 1.97 eV, Figure 5.25(a). This high energy band gap could be due to the presence of ZnS and $CuSnS_3$ as seen in quality determination using Raman spectroscopy, Figure 5.28. This high band gap could also be due to other phases present in CZTS at this annealing temperature and some defects (Sheng *et al*., 2012).

The band gap of CZTS after annealing in nitrogen gas at 500^{o}C under sulphur vapor was found to be 1.69 eV, Figure 5.25(b). This high energy band gap was due to the presence of ZnS and $CuSnS_3$ according to the quality determination from Raman Spectroscopy (Tiong *et al*., 2014).

The band gap of CZTS after annealing in nitrogen gas at 550^{o}C under sulphur vapor was found to be 1.59 eV, Figure 5.25(c), and is within the CZTS band gap range according to other studies which is 1.51 - 1.76 eV (Pawar *et al.,* 2011). The best band gap was expected at approximately 1.45 eV but this was not possible due to the presence of ZnS in the film according to the quality determination using Raman spectroscopy. This is according to the value from other studies ([a]Shinde *et al.,* 2013).

According Figure 5.25(d), the band gap of CZTS varied with annealing temperature, that is, it decreased with increase in annealing temperature up to an optimum annealing temperature of 550^{o}C. It was not possible to know what could happen to the band gap above 550^{o}C since the samples sublimed at temperatures above 550^{o}C.

The reduction of band gap with annealing temperature was as a result of significant transformation of the binary phases and the formation of crystalline CZTS (Pawar *et al*., 2014). For example from Raman peaks diagrams, section 5.7.1.6, it is observed that at 550^{o}C only a small peak of ZnS appears. The band gap obtained was still within the desired optimum range (Sheng *et al*., 2012). Other researchers have tried etching using toxic KCN to get rid of ZnS completely from their samples (Tiong *et al.,* 2014), which was to ensure that a band gap range of between 1.41 - 1.51 eV was obtained. Based on this study and theoretical knowledge, it is without doubt that band gap depends very much on the impurities in the film as well as secondary phases and annealing temperatures. Band gap also reduces due to increase in grain size at high annealing temperatures (Tumuluri *et al*., 2012).

5.7.1.4 Absorption Coefficient of Annealed CZTS Film Deposited by Layering Method Followed by Chemical Bath in Na_2S Solution

In the short wavelength region where reflectance was very low as was the case of highly structured surface, the absorption coefficient was calculated using the formula:

$$\alpha = -\frac{1}{d}\ln\left(\frac{1}{T_{norm}}\right) \tag{5.10}$$

where α, *d*, and T_{norm} are defined in section 3.1.

The variation of absorption coefficient with energy is in the Figure 5.26. It is observed that absorption coefficient is in the range of ~10^4 to ~10^5 cm^{-1}withinthe region ≥1.50 eV. The high value of absorption coefficient obtained in this study was within the range observed in other studies (Singh *et al.*, 2015). This high absorption coefficient implies that the intensity of light transmitted is low and hence the high absorption in this region, ≥1.50 eV. This high absorption improves the cell's efficiency and thus makes CZTS thin film materials a promising replacement for CIGS thin film technologies. In addition a thin film semiconductor is considered suitable material for photovoltaic solar energy conversion if the absorption coefficient is larger than 10^4 cm^{-1} (Singh *et al.*, 2015), which is clearly the case with the CZTS film made.

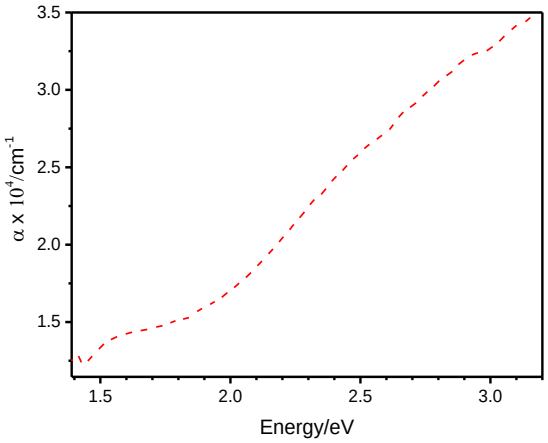

Figure 5.26: The absorption coefficient of annealed CZTS deposited by layering method followed by chemical bath in Na_2S annealed at 550°C

5.7.1.5 Electrical Characterization of CZTS Film Deposited in Layers

Electrical characterization was done using four point probe system, Guardian (SRM-232-100). The volume electrical resistivity of the films annealed at different temperatures was calculated as follows: Sheet resistance (ohms-per-square) multiplied by the thickness of the material in centimeters, equals the volume resistivity (ohms-cm). Summary of the electrical characterization is shown in table 5.1.

Table 5.1: Variation of film thickness, sheet resistivity and volume resistivity with temperature.

Temperature (^oC)	Film Thickness (cm)	Sheet Resistivity (Ω/square)	Volume Resistivity (Ωcm)
450	1.89×10^{-5}	13.22	2.50×10^{-4}
500	3.90×10^{-5}	10.22	4.00×10^{-4}
550	6.20×10^{-5}	9.22	5.70×10^{-4}

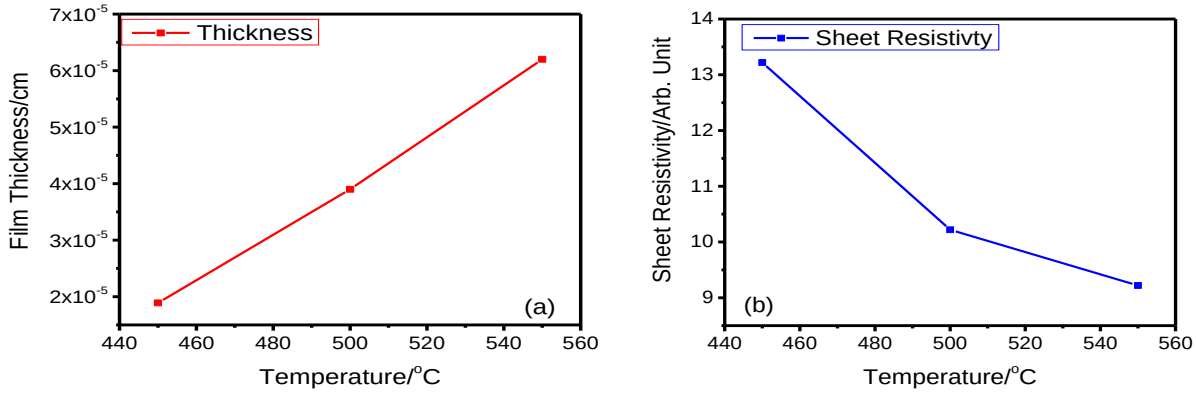

Figure 5. 27: (a) Thickness variation with annealing temperature (b) Sheet resistivity variation with temperature.

The observed volume electrical resistivity of the annealed sample was in the order of 10^{-4} Ω cm which was comparable to other researchers' work ([a]Shinde *et al.*, 2013). The decrease in sheet resistivity with annealing temperature, Table 5.1 and Figure 5.27, is because of grain size increase which increases with the annealing temperature ([b]Shinde *et al.*, 2013).

5.7.1.6 Quality Determination of CZTS Film Deposited in Layers using Raman Spectroscopy

The shape and position of Raman peaks are strongly influenced by the presence of defects in the sample, either in the form of structural inhomogenities or secondary phases. Typical Raman spectra for CZTS films are given in Figure 5.28 – 5.30.

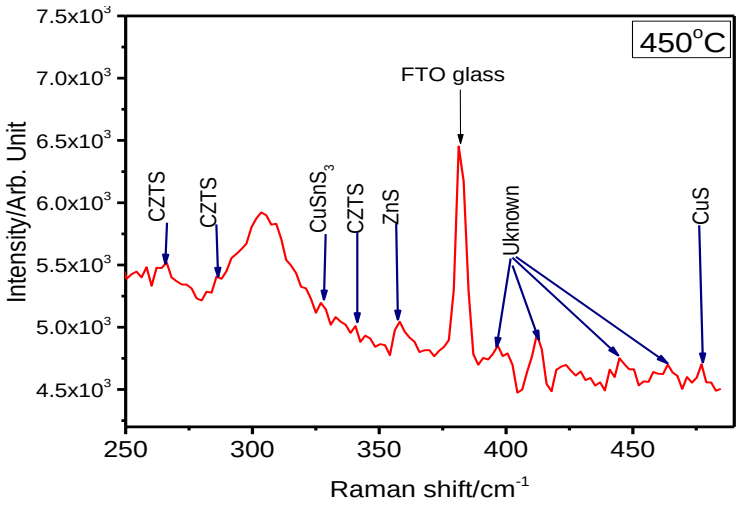

Figure 5. 28: Raman peaks of CZTS film deposited by layering method followed by chemical bath in Na_2S solution annealed at 450°C.Laser 785 nm, exposure time 10 s, number of accumulations 5 s, objective ×50 and intensity 50%.

Several Raman peaks were observed at 266 cm^{-1}, 287 cm^{-1}, 334 cm^{-1}, 333 cm^{-1}, 359 cm^{-1}, and 477 cm^{-1} for sample annealed at 450°C. Of these peaks, three peaks at 266 cm^{-1}, 286 cm^{-1} and one at 341 cm^{-1} were identified to be CZTS as shown in the spectrum. The 359 cm^{-1} peak is attributed to ZnS binary phase while 477 cm^{-1} peak was due to CuS. Similar observations had been reported by Dimitrievska *et al.*, (2014). These peaks could be due to other binary and ternary produced during the formation of CZTS film.

In Figure 5.29, the intensities of ZnS and CuS were reduced in sample annealed at 500°C compared to those annealed at 450°C.

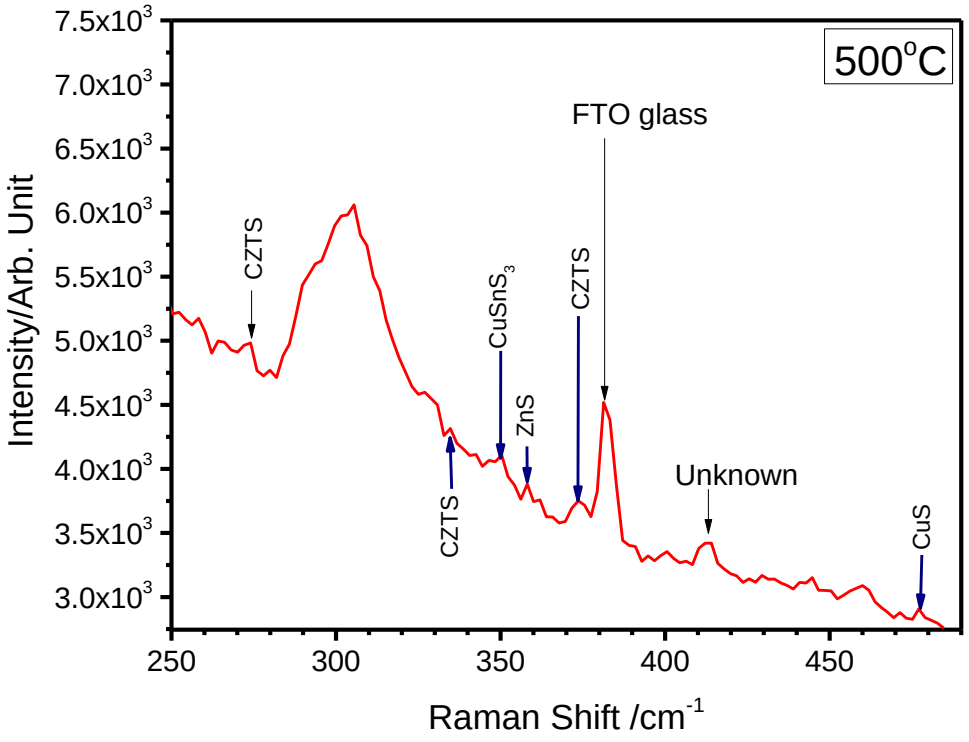

Figure 5.29: Raman peaks of CZTS film deposited by layering method followed by chemical bath in Na_2S solution annealed at 500°C.

From Figure 5.29, the Raman peaks observed at 335 cm^{-1}, 351 cm^{-1}, 356 cm^{-1} 373 cm^{-1} and 475 cm^{-1} were for the sample annealed at 500°C. The peaks at 335 cm^{-1} and 373 cm^{-1} peaks were as a result of CZTS structure, while those at 356 cm^{-1}, 351 cm^{-1} and 475 cm^{-1} were as a result of ZnS, $CuSnS_3$ and CuS phases respectively.

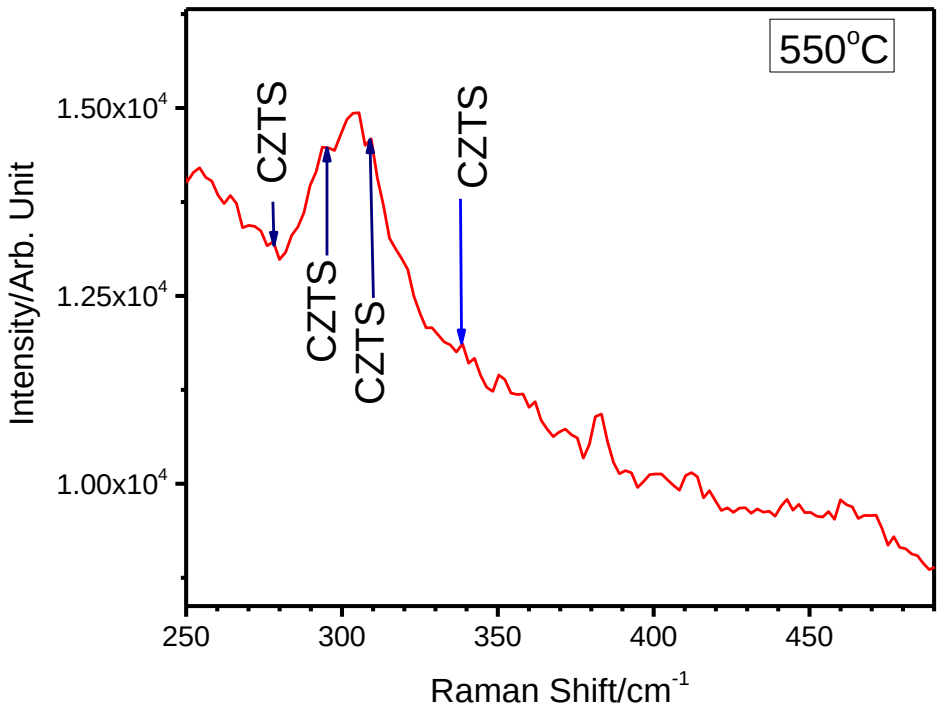

Figure 5.30: Raman peaks of CZTS film deposited by layering method followed by chemical bath in Na_2S solution annealed at 550°C. Laser 785 nm, exposure time 10 s, number of accumulations 5 s, objective ×50 and intensity 50%.

From Figure 5.30, the Raman peaks were observed at 278 cm^{-1}, 293 cm^{-1}, 310 cm^{-1} and 338 cm^{-1} were for sample annealed at 550°C under the flow of nitrogen gas. The peaks at 278 cm^{-1}, 293 cm^{-1}, 310 cm^{-1} and 338 cm^{-1} were attributed to CZTS crystalline structure (Dimitrievska *et al.*, 2014, Lydia and Reddy, 2013).

The shift in the main CZTS peak position which were 333 cm^{-1}, 335 cm^{-1} and 337 cm^{-1} for samples annealed at 450°C, 500°C and 550°C respectively could be due to local inhomogeneities with high degree of disorder in the cation of sublatice of CZTS film and the wavelength of laser excitation used which was 785 cm^{-1}. There was a very small peak at 256 cm^{-1} which was an indicator of the presence of ZnS. The presence of ZnS in the sample annealed at 550°C indicated that the CZTS thin film deposited was rich in Zn (Dimitrievska *et al.*, 2014) as expected for a best performing CZTS film. Zn rich prevents formation of Cu-Sn-

S ternary phases, which was readily converted to CZTS under heat treatment (Singh *et al.*, 2015).

The intensities of optical Raman modes of CZTS could vary depending on the excitation wavelength of the sample. Raman modes such as 302.1 cm^{-1} which has not been identified by researchers could be due to low intensities produced by the excitation wavelength chosen (Dimitrievska *et al.*, 2014).

5.7.2 CZTS Film Deposited using co-electrodeposition of CZT Followed by Chemical Bath in Na_2S Solution

5.7.2.1 Optical properties of As-deposited CZTS Film deposited using co-electrodeposition of CZT followed by Chemical Bath in Na_2S Solution

Transmittance and reflectance of as-deposited CZTS deposited using co-electrodeposition of CZT followed by chemical bath in Na_2S solution was as shown in Figure 5.31.

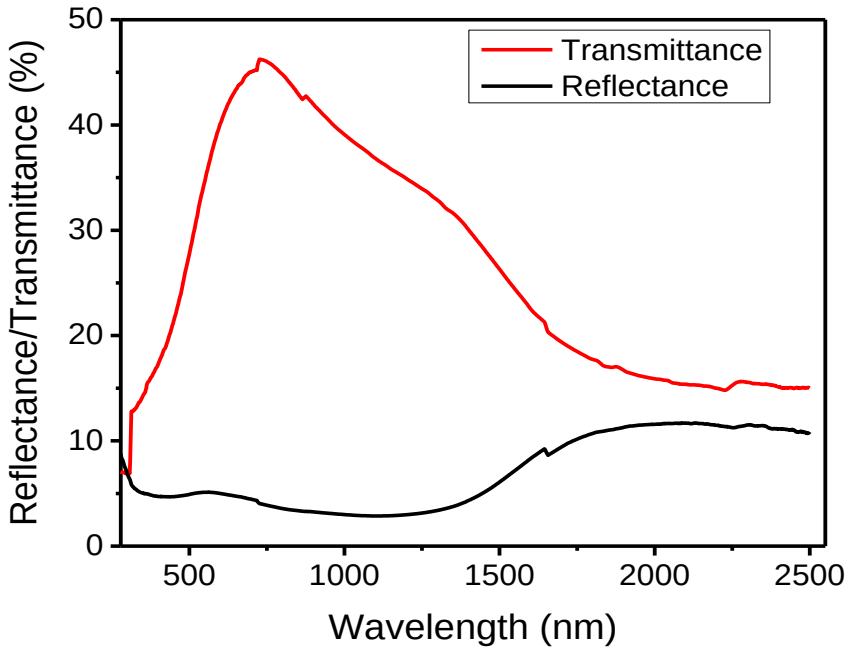

Figure 5.31: Transmittance and reflectance of as deposited CZTS deposited by use of co-electrodeposition of CZT followed by chemical bath in Na_2S.

The transmittance of the as-deposited CZTS as per Figure 5.31 was observed to be high in the visible region, 45%. Transmittance dropped rapidly in the long wavelength/near infrared region, which was expected but not very much as it is. The drop could be due to the TCO coating on the substrate used. This behavior of the film of this thickness apart from being applied in photovoltaics, it can be used as smart windows, to cut away the dangerous infrared and ultraviolet rays.

The reflectance of the film from the Figure 5.31 was very low, 5%. The low reflectance is very important for films meant for photovoltaic application since it ensures that maximum light enters the film. This enhances conversion efficiency of solar cells. From $R+A+T=100\%$ and the values of T and R above, A which is absorbance of the film is approximately 50% which is a good value for an absorber layer.

5.6.2.2 Band Gap of As-deposited CZTS Film deposited using co-electrodeposition of CZT followed by Chemical Bath in Na_2S Solution

The band gap of as-deposited CZTS film deposited by co-electrodeposition of CZT followed by chemical bath in Na2S solution was approximated as shown in Figure 5.32.

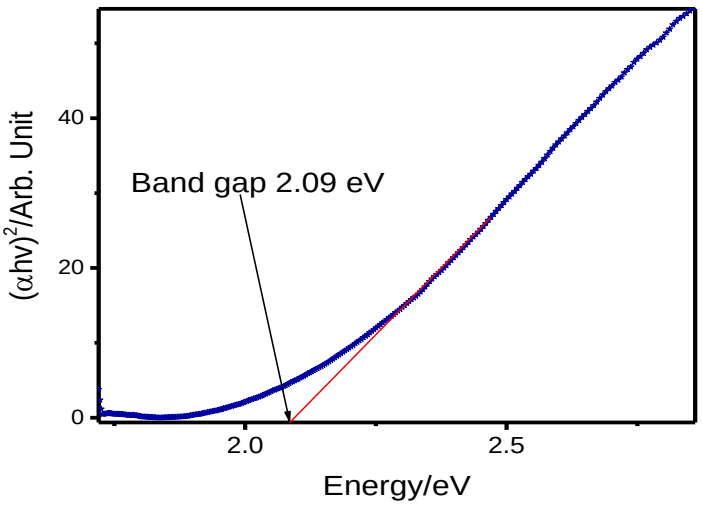

Figure 5.32: Band gap of as-deposited CZTS deposited by use of co-electrodeposition of CZT followed by chemical bath in Na_2S.

The band gap of as deposited CZTS was found to be 2.09 eV. This was a high value because before annealing the film was amorphous and contained the secondary phases like CuS, SnS and ZnS (Tiong *et al*., 2014).

5.7.2.3 Optical Properties of Annealed CZTS Film Deposited Using Co-Electrodeposition of CZT followed by Chemical Bath in Na_2S Solution

Transmittance and reflectance graphs of CZTS deposited by co-deposition of CZT followed by chemical bath in Na_2S solutions annealed at different temperatures were as shown in Figure 5.33.

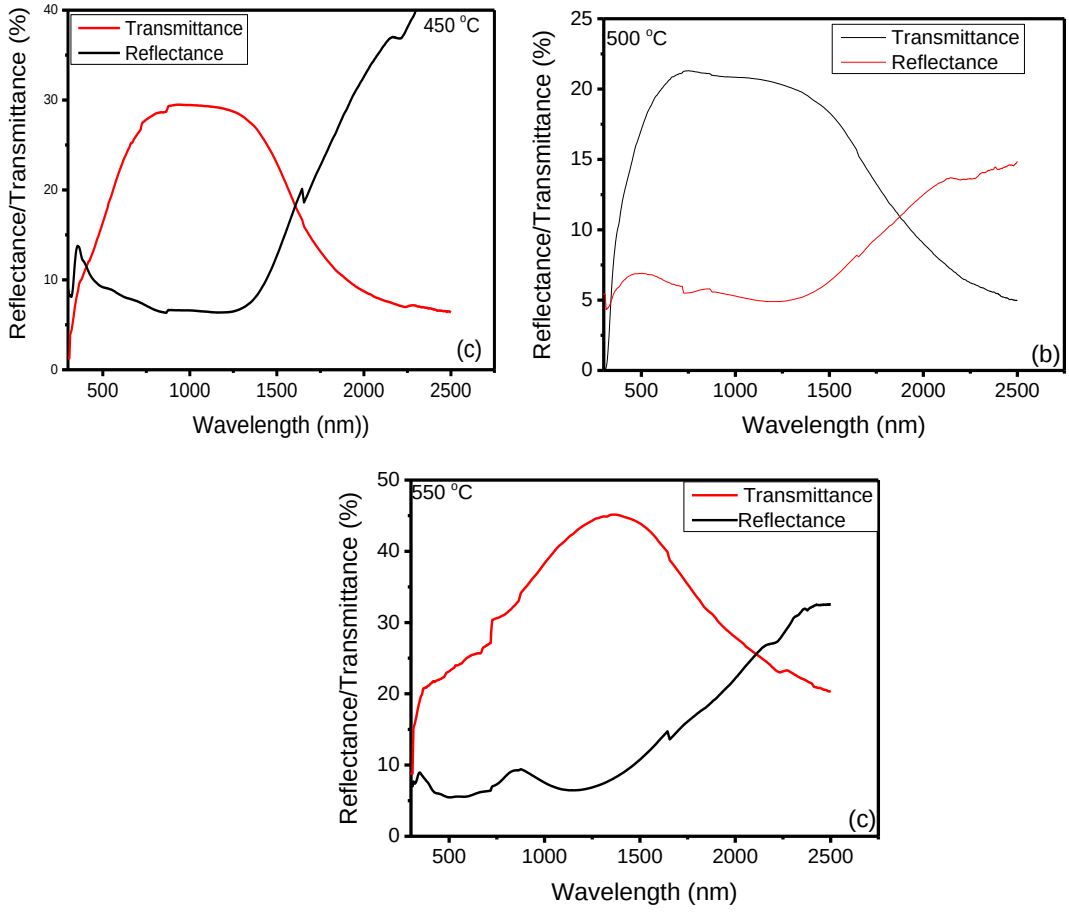

Figure 5.33: Transmittance and reflectance of CZTS deposited by use of co-electrodeposition of CZT followed by chemical bath in Na_2S annealed at;(a) 450°C, (b) 500°C and (c) 550°C.

According to Figure 5.33, transmittance of annealed CZTS prepared by co-electrodeposition followed by chemical bath was generally 25% for all the annealing temperatures in the visible region. Reflectance of the sample was generally low in the visible wavelength region implying that a large percentage of light incident on such CZTS surface would either be transmitted or absorbed. But since transmittance was low in this region, this implies that approximately 70% of light in the visible region will be absorbed by a CZTS thin film.

5.7.2.4 Band Gap of Annealed CZTS Film Deposited using Co-electrodeposition of CZT followed by Chemical Bath in Na_2S Solution

Band gap approximation graphs of annealed CZTS deposited using co-electrodeposition of CZT followed by chemical bath in Na_2S solution is presented in Figure 5.34.

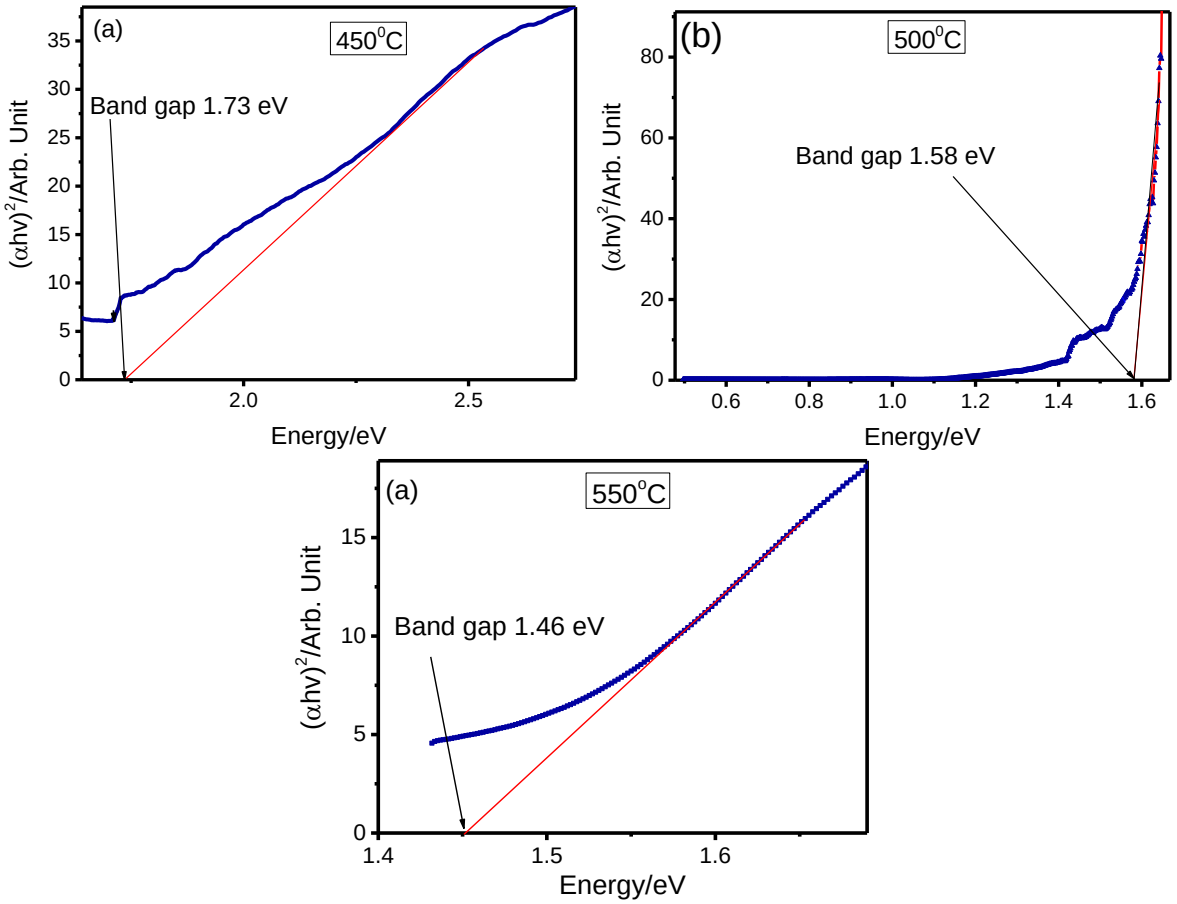

Figure 5.34: Band gap of CZTS deposited by use of co-electrodeposition of CZT followed by chemical bath in Na_2S annealed at; (a) 450°C, (b) 500°C and (c) 550°C

The band gap of the films annealed at 450°C and 500°C were observed to be 1.71 eV and 1.60 eV, respectively. These high band gaps could be due to other phases which are present in the sample as seen in the Raman spectrum of these films, section 5.2.27. The band gap of the film annealed at 550°C was observed to be 1.46 eV; which is within the range that have been achieved by other researchers at this temperature (Septina *et al.*, 2013) which ranged between 1.00 - 1.50 eV.

Since the efficiency of CZTS solar cells having Cu-poor and Zn-rich favours the growth of other phases during formation of the film (Hossain, 2012), secondary phases are expected, but because sulfur was in plenty all the secondary phases contain sulphur. Since Cu_xS has a direct

band gap range of 1.7 - 2.1 eV that varies with the values of x, the increased band gap could be due to Cu_xS phases and other secondary phases present in the film. ZnS, SnS_2 and Cu_2SnS_3 occur easily under lower growth temperatures during annealing process (Sheng *et al*., 2012). Cu_2SnS_3 is detrimental in the film because it is not easy to convert to quaternary structure unlike the binary phases which readily converts to quaternary structure under temperature treatment (Singh *et al*., 2015).

From the band gap data and Raman data it was observed that other phases and impurities affect band gaps of CZTS films, section 5.7.2.4 and 5.7.2.7. The band gap values of the samples decreased upon increasing annealing temperature, this could have been due to elimination of other phases having higher band gaps (Tiong *et al*., 2014). In addition, as annealing temperature increases there is evidence of grain size growth, and since band gap energy is inversely proportional to the size of nanoparticles, small band gap energy is expected for high annealing temperatures as seen (Tumuluri *et al*., 2012).

5.7.2.5 Absorption Coefficient of CZTS Deposited using Co-electrodeposition of CZT followed by Chemical Bath in Na_2S Solution

The result of variation of absorption coefficient against energy was shown in the Figure 5.40. From Figure 5.35, it was observed that absorption coefficient is above 10^4 cm^{-1} in the entire range considered. This value of absorption coefficient was in accordance to other studies on absorption coefficient of CZTS (Shin *et al*., 2011).

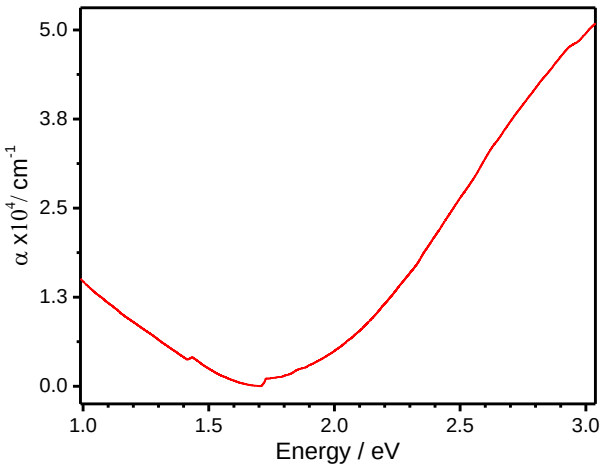

Figure 5.35: Absorption coefficient variation with photon energy.

5.7.2.6 Electrical Characterization of CZTS Deposited Using Co-electrodeposition of CZT followed by Chemical Bath in Na_2S Solution

The volume electrical resistivity of the films annealed at different temperatures was calculated as follows: Sheet resistance (ohms-per-square) multiplied by the thickness of the material in centimeters, equals the volume resistivity (ohms-cm).

Table 5.2: Summary of variation of film thickness, sheet resistivity and volume resistivity with temperature.

Temperature (^{0}C)	Film Thickness (cm)	Sheet Resistivity (Ω/square)	Volume Resistivity (Ωcm)
450	5.50×10^{-6}	13.22	7.27×10^{-5}
500	1.00×10^{-5}	10.00	1.00×10^{-4}
550	2.00×10^{-5}	9.89	1.98×10^{-4}

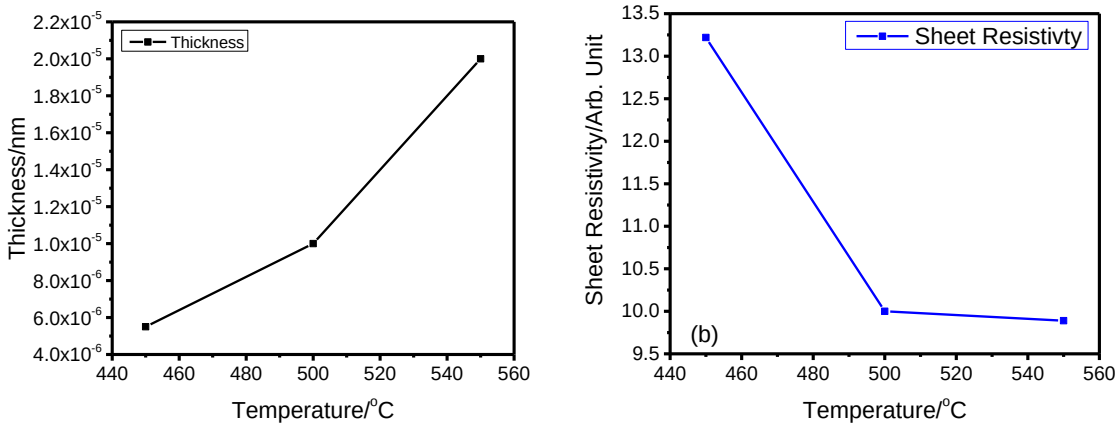

Figure 5.36**:** (a) Thickness variation with annealing temperature (b) Sheet resistivity variation with temperature.

From Table 5.2 and Figure 5.36, it is observed that, the sheet resistivity increases with increase in annealing temperature. This is because as annealing temperature increases there is an increase in grain size of CZTS grains, this is evident as seen in Figure 5.36(a). This result is in accordance to other experimental observations (Sheng *et al*., 2012)

From this data of electrical characterization it was observed that the volume electrical resistivity of the annealed sample is in the order of 10^{-4} Ω cm which is slightly lower than the predicted value which is in the order of 10^{-3} Ω cm (Shinde *et al.*, 2012). This difference could be due to difference in film thickness or composition (Sheng *et al* 2012).

5.7.2.7 Quality Determination of CZTS Film Deposited using Co-Electrodeposition of CZT followed by Chemical Bath in Na_2S Solution using Raman Spectroscopy

By sampling random areas of the thin films annealed at different temperatures that was 550ºC, 500ºC and 450ºC, typical Raman spectra for CZTS given in Figure 5.37– 5.39 were collected..

In Figure 5.37, Raman peaks were observed at 276 cm^{-1}, 310 cm^{-1}, 335 cm^{-1}, 349 cm^{-1}, 358 cm^{-1} and 475 cm^{-1} for sample annealed at 450ºC under the flow of nitrogen gas. The 276 cm^{-1}, 310 cm^{-1} and 335 cm^{-1} peaks were as a result of CZTS structure, while those at 349 cm^{-1}, 358 cm^{-1} and 475 cm^{-1} peaks was as a result of ZnS, $CuSnS_3$ and CuS respectively. These results were in agreement with other works (Dimitrievska *et al.*, 2014).

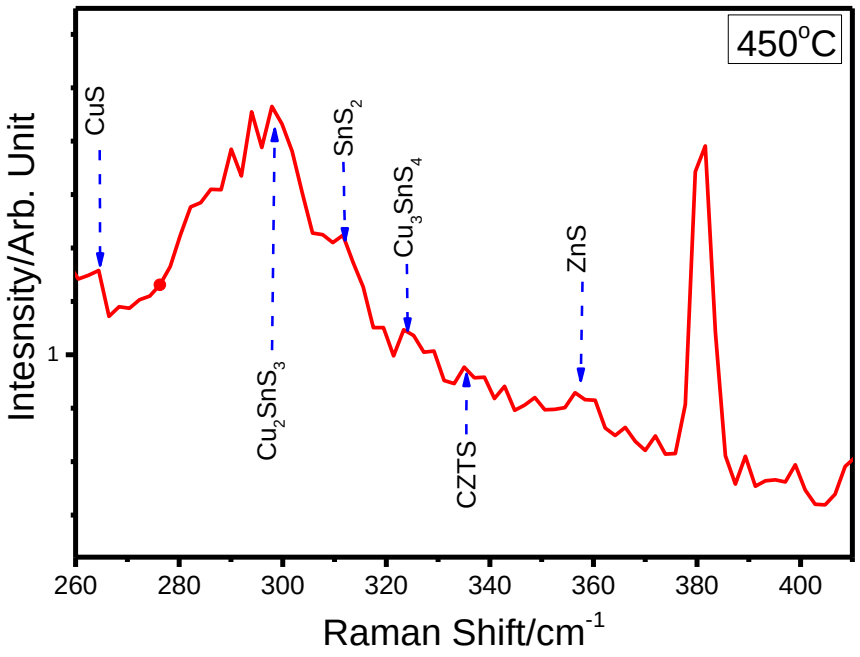

Figure 5.37: Raman peaks of CZTS deposited by Co-electrodeposition method followed by chemical bath in Na_2S solution annealed at 450°C. Laser 785 nm, exposure time 10 s, number of accumulations 5 s, objective ×50 and intensity 50%.

In Figure5.38, Raman peaks were observed at 265 cm^{-1}, 297 cm^{-1}, 313 cm^{-1}, 322 cm^{-1}, 337 cm^{-1} and 356 cm^{-1} for sample annealed at 500°C under the flow of nitrogen gas. Peak 337 cm^{-1} was as a result of CZTS structure; 297 $cm^{-1}$was due to Cu_2SnS, 313 cm^{-1} could be due to SnS_2, 322 cm^{-1} could be due to Cu_3SnS_4 and 356 cm^{-1} peak was due to ZnS. These results were in agreement with other works (Dimitrievska *et al.*, 2014). These secondary and ternary phases in CZTS annealed at 500°C were responsible for its large band gap. ZnS intensity was high in samples annealed at 450°C as compared to sample annealed at 500°C. Other unknown peaks were also observed in the Raman spectra of the sample annealed at 450°C as compared to samples annealed at 500°C, this peaks could be due to other binary and ternary phases in CZTS formed.

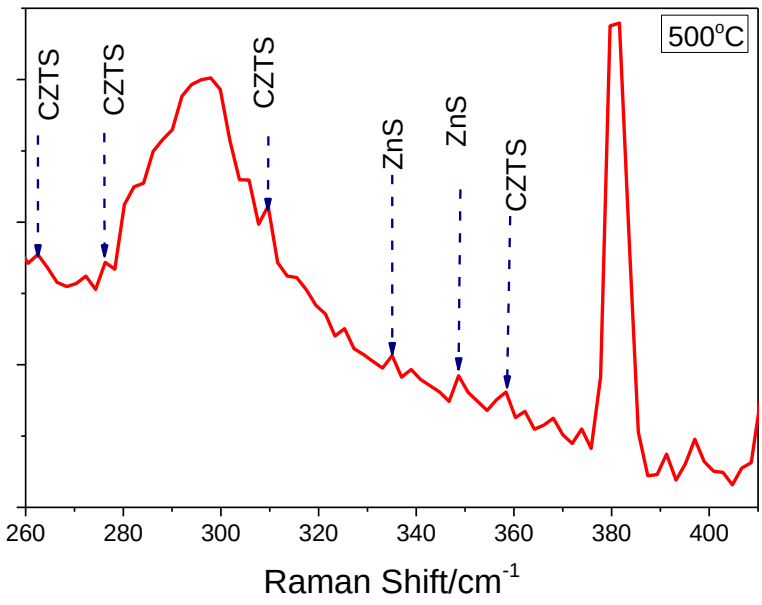

Figure 5.38: Raman peaks of CZTS deposited by Co-electrodeposition method followed by chemical bath in Na_2S solution annealed at 500°C. Laser 785 nm, exposure time 10 s, number of accumulations 5 s, objective ×50 and intensity 50%.

According to Figure 5.39, Raman peaks were observed at 261 cm^{-1}, 288 cm^{-1}, 338 cm^{-1} and 368 cm^{-1} for sample annealed at 550°C under the flow of nitrogen gas. The peaks at 261 cm^{-1}, 288 cm^{-1}, 338 cm^{-1} and 368 cm^{-1} were attributed to CZTS structure (Dimitrievska *et al.*, 2014, Lydia and Reddy, 2013). From the two peaks which specifically represent CZTS, it is clear that CZTS deposited and annealed in this manner was pure and best for application in solar cells. At annealing temperature of 550°C no secondary phases were observed, this implied that secondary phases could be removed by heat treatment.

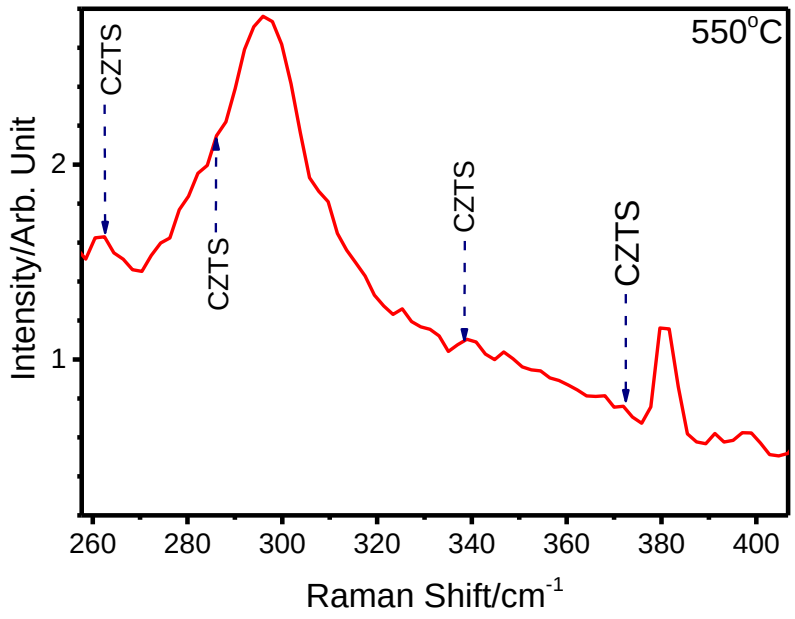

Figure 5.39: Raman peaks of CZTS deposited by Co-electrodeposition method followed by chemical bath in Na_2S solution annealed at 550°C. Laser 785 nm, exposure time 10 s, number of accumulations 5 s, objective ×50 and intensity 50%.

5.7.2.8 Summary of Raman peaksand band gaps of CZTS Film Deposited using Co-Electrodeposition of CZT followed by Chemical Bath in Na_2S Solution.

Table 5.3: Effect of annealing temperature on the Raman peaks and optical band gaps of the deposited CZTS films

Annealing Temperature /°C	Raman Peak / cm^{-1}	Optical band gap / E_g (eV)
550	338	1.45
500	337	1.60
450	335	1.71

From table 5.3, the peak shift in Raman spectra predicted the improvement in the crystallinity of CZTS phase (Singh *et al.*, 2015 and Mkawi *et al.*, 2013) at higher annealing temperature. These changes in the Raman peak positions and broadening could be due to the variation in the crystallite size. Optimizing the annealing temperature was therefore important in obtaining crystallized and pure CZTS film.

The band gaps were steadily reducing with annealing temperature as observed from table 5.3 with the best band gap being observed at annealing temperature of 550^{o}C. This showed that during annealing at higher temperatures other phases present in CZTS which could result in band gap increment are converted to form pure CZTS with the best band gap.

5.8 Comparison between CZTS Film Deposited in Layers and CZTS Deposited by Co-Electrodeposition

Table 5.4: Comparison of the properties of CZTS film deposited in layers and that deposited by co-electrodeposition followed by chemical bath

	CZTS depositedin layers			CZTS Deposited by Co-electrodeposition		
Annealing Temperature (^{o}C)	550	500	450	550	500	450
Raman Peak (cm^{-1})	338	335	333	338	337	335
Optical band gap, E_g (eV)	1.59	1.70	1.97	1.45	1.60	1.71

.

Assumption taken during comparison; the films thicknesses were uniform. From table 5.4, the peak shift in Raman spectra showed that in both cases crystallinity of the sample improved with increase in annealing temperature. These changes in the Raman peak positions and broadening could be due to the variation in the crystallite size which varies with annealing

temperature. Optimizing the annealing temperature was therefore important in obtaining crystalline and pure CZTS as observed from the Raman shifts diagrams.

From table 5.4, apart from band gap varying with temperature in each case, it is observed at each temperature the band gap of CZTS film deposited by co-electrodeposition followed by chemical bath in Na_2S solution is lower than that of CZTS deposited in layers followed by chemical bathNa_2S solution. This disparity could be due to difference in homogeinity of the films thicknesses ([a]Shinde *et al*., 2013).

CHAPTER SIX: CONCLUSIONS AND RECCOMENDATIONS FOR FARTHER WORK

6.1 Conclusions

Copper zinc tin sulphide (CZTS) thin film technology can be used as a substitute to the already existing thin film solar technology, copper indium gallium selenide (CIGS), since CZTS technology is a non-toxic, earth abundant materials and cheap technology. The main aim of this study which was to deposit CZTS thin films using electrodeposition coupled with chemical bath to develop low cost solar cell absorber layer has been achieved.

The first specific objective which was to evaluate the electrical and optical properties of CZTS thin films deposited by cathodic sweep electro-deposition coupled with chemical bath deposition techniques has been achieved and this is evidence in results and discussion chapter.

The second specific objective which was to evaluate the effect of annealing temperature on CZTS thin films optical and electrical properties was achieved. The band gap of the CZTS films deposited by layering method followed by chemical bath in sodium sulphide solution were 1.59 eV, 1.70 eV and 1.97 eV for samples annealed at 550^{o}C, 500^{o}C and 450^{o}C,respectively. The band gaps of films deposited by co-electrodeposition followed by chemical bath in sodium sulphide solution were 1.46 eV, 1.60 eV and 1.71 eV for annealing temperatures of 550^{o}C, 500^{o}C and 450^{o}C respectively. From these band gap values it is concluded that band gap is inversely proportional to annealing temperature, within the investigated range of temperatures, 550^{o}C, 500^{o}C and 450^{o}C. The lowest and best band gap of CZTS film is obtained at annealing temperature of 550^{o}C. In addition, samples deposited by co-electrodeposition followed by chemical bath in sodium sulphide solution produced the best band gap at 550^{o}C, 1.46 eV, which is close to the optimum band gap of a high efficient thin film band gap which is 1.35 eV (Ananthan and Mahalaskmi, 2014). The electrical properties of the film were evaluated and it was found that the sheet resistivity was decreasing with increase in annealing temperature. The volume resistivity was in the order of 10^{-4} Ωcm for all

the annealing temperatures investigated. This was a good value as it was in the range reported in other studies (Shinde *et al.*, 2012)

The third specific objective which was to determine the structure of the deposited CZTS film using Raman spectrophotometer was achieved. After annealing of the deposited samples at temperature of 550^{o}C, it was observed that the desired CZTS structure was formed. This was shown by Raman spectroscopy, which showed the main vibrational modes of CZTS at 288 cm^{-1}, 338 cm^{-1} and 368 cm^{-1}. This shows that the formation of secondary phases which were seen at lower annealing temperatures of 450^{o}C and 500^{o}C can be suppressed by increasing annealing temperatures to 550^{o}C.

6.2 Recommendations for Farther Work

- More research work to be done on co-electrodeposition method in order to attain accurate reduction and oxidation potential of the combined metals.
- The band gap of CZTS film has been obtained in this study experimentally, the interaction of the band gap of individual sulphide metals i.e. CuS, SnS and ZnS to produce the small band gap of 1.45 eV needs to be investigated farther.

Reference

Ahmed S., Reuter K. B., Gunawan O., Guo L., Romankiw L. T. and Deligiani H., (2011), A high efficiency electrodeposited Cu_2ZnSnS_4 solar cell, *Advanced Energy Materials*, **20,** 1-7

Ananthan M. R. and Mahalaksmi B., (2014), Review on CZTS based solar cells, *Advances in Natural and applied sciences*, **8**(21) 72-75

Araki H., Kubo Y., Jimbo K., Maw S. W., Katagiri H., Yamazaki M., Oishi K. and Takeuchi A., (2009), Preparation of Cu_2ZnSnS_4 thin films by sulfurization of co-electroplated Cu-Zn-Sn precursors, *Phys. Status Solidi c*, **6**(5) 1266-1268

Artemyev D., Zakharov V., Bratchenko I. Myakinin O., Kozlov S. and Moryatov A., (2014), Combined Raman spectroscopy & autoflourescence method for tumors research, *Saratov Full meeting symposium*: Optics & biophotonics

Borah J. P. and Sarma K. C., (2008), Optical and optoelectronic properties of ZnS nanostructured thin film, *ActaPhysicaPolonica A*, **114** (4) 713-719

Callister W. D. Jr., (2007), Materials science and engineering an introduction, *John Wiley and Sons, Inc*, Seventh edition page W57-W71

Chen S., Gong X. G., Walsh A. and Wei S., (2009), Crystal and electronic band structure of Cu_2ZnSnX_4 (X=S and Se) photovoltaic absorbers: First-principles insights, *Applied Physics Letters*, **94**, 041903 1-3

Cheng L. L., Liu M. H., Wary M. X., Wary S. C., Wary G. D., Zhou Q. Y. and Chen Z. Q., (2012), Preparation of SnS films using solid sources deposited by PECVD method with controllable film characters, *Journal of Alloys and Compounds, **545*** 122-129

Dhasade S. S., Patil J. S., Thombare J. V. and Fulari J. V., (2015), Studies on synthesis and characterization of copper sulfide thin films, *Journal of Shiraji University (Science and Technology)*, **4** (2) 1-3

Dimitrievska M., Fairbrother A., Fontane X., Jawhari T., Izquierdo-Roca V., Saucedo E. and Perez-Rodriguez A., (2014), Multiwavelength excitation Raman scattering study of polycrystalline kesterite Cu_2ZnSnS_4 thin films, *Applied Physics Letters*, **104** 021901 (5pp)

Dolgonos A., Mason T. O. and Poeppelmeier K. R., (2016), Direct optional band gap measurement in polycrystalline semiconductors: A critical look at the Tauc method, *Journal of solid state chemistry*, **240** 43-48

Fernandes P. A., Salome P. M. and Cuhna A. F., (2011), Study of polycrystalline Cu_2ZnSnS_4 films by Raman scattering, *Journal of alloys and compounds*, **509** 7600-7606

Fernandes P. A., Salome P. M. P., Cuhna A. F. and Schubert B. A., (2010), Cu_2ZnSnS_4 solar cells prepared with sulphurized dc-sputtered stacked metallic precursors, *Thin Solid Films* **519** 7382-7385

Freeda M. A., Mahadevan C. K. and Ramalingom S**.,** (2011), Optical and electrical properties of CuSnanorods, *Scholars Research Library*, **2** (3) 175-179

Guo Q., Ford G. M., Yang W. C., Walker B. C., Stach E. A., Hillhouse H. W. and Agrawal R., (2010), Fabrication of 7.2% efficient CZTSSE solar cells using CZTS nanocrystals, *J. A.M chemical society* **132** 17384-17386

Guo L., Zhu Y., Gunawan O., Gokmen T., Deline V. R., Ahmed S., Romankiw T. and Deligianni H., (2014), Electrodeposited $Cu_2ZnSnSe_4$ thin film solar cell with 7% power conversion efficiency, *Progress in Photovoltaics research and applications*, **22** 58-68

Grujicic D. and Pesic B., (2002), Electrodeposition of copper; the nucleation mechanisms, *Electronic Acta*, **47** 2901-2912

Hedge S. S., Kunjumana A. G., Ramesh K., Chandrasekharan K. A. and Pranshantha M**.,** (2011) Preparation and characterization of SnS thin films for solar cell application, *International Journal of Soft Computing and Engineering*, **1**1-3

Hiroi H., Sakai N. and Sugimoto H.,(2011), Cd-free 5×5cm^2-sized Cu_2ZnSnS_4sub modules, *37th IEE Photovoltaic Specialists Conference (PVSC)* 2719-2722

Holdren P. J., (1991), Population and energy problems, **12**(3) 240

Hossain M. I**.,** (2012), Prospects of CZTS solar cells from the perspective of material properties, fabrication methods and current research challenges, *Chalcogenide Letters*, **9**(6) 231-242

Ito K. and Nakazawa T., (1988), Electrical and optical properties of stannite-type quaternary semiconductor thin films, *Japanese Journal of Applied Physics*, **27**(part 1, No. 11) 2094-2097

Jiang M. and Yan X**.,**(2013), Cu_2ZnSnS_4 Thin Film Solar Cells: Present Status and Future Prospects, *INTECH (opensource/openminds), Chapter 5*

Just J., Lutzenkirchen-Hecht D., Frahm R., and Schorr S., (2011), Determination of secondary phases in kesteriteCu_2ZnSnS_4 thin films by x-ray absorption near edge structure analysis, *Applied Physics Letters*, **99**, 262105, 1-3

Kanuru S. C., Shekar G. L., Krishnamurthy L., Urs R. G. K., (2014), Surface morphological studies of solar absorber layer Cu_2ZnSnS_4 (CZTS) thin films by non-vacuum deposition methods, *Journal of Nano-and Electronic Physics*, **6**(2) 02004(5pp)

Katagiri H., Jimbo K., Yamada S., Kamimura T., Maw W. S., Fukano T., Ito T. and Matohiro T., (2008), Enhanced conversion efficiencies of Cu_2ZnSnS_4-based thin film solar cells by using preferential etching technique, *Applied Physics Express*, **1**(4) 1-2

Kato T., Hiroi H., Sakai N., Muraoka S. and Sugimoto H., (2012**)**, Characterization of front and back interfaces on Cu_2ZnSnS_4 thin film solar cells, *Proceedings of 27thEU PV SEC*, 2236-2239

Kittel C., (2005), Introduction to solid state physics, John Wiley and Sons, Inc, Eighth edition page 430

Lydia R. and Reddy S. P**.,** (2013), Structural and optical properties of Cu_2ZnSnS_4 nanoparticles for solar cell applications, *Journal of Nano- and Electronic Physics*, **5**(3) 03017(4pp)

Mane R. S. and Lokhande C. D., (2000), Chemical deposition method for metal chalcogenide thin films: Review, *Materials Chemistry and Physics*, **65** 1-31

Mau T.T. and Kim K. H., (2012), Synthesis of Cu_2ZnSnS_4 thin film absorbers by sulfurizing dip-coated precursors, *Journal of Ceramic Processing Research*, **13**(3) 301-304

Mendoza-Huizar L. H., Ries-Reyes C. H., and Gomez-Villegas M. G**.,** (2009), Zinc electrodeposition from chloride solutions onto glassy carbon electrode, *Journal of Mexican Society*., **55**(4) 243-247

Millazo G., Caroli S. and Sharma V. K., (1978), Tables of standard electrode potentials, Wiley, Chichester

Mkawi E. M., Ibrahim K., Ali M. K. M., Farrukh M. A. and Mohamed A. S., (2013), Synthesized and characterization of Cu_2ZnSnS_4 (CZTS) thin films deposited by electrodeposition method, *Applied Mechanics Materials* **343** 85-89

Pawar B. S., Pawar S. M., Gurav K. V., Chin S. W., Lee J. Y., Kolekar S. S. and Kim J. H., (2011), Effect of annealing atmosphere on the properties of electrochemically deposited Cu_2ZnSnS_4 (CZTS) thin films, *International Scholarly Research Network-Renewable Energy*, Article ID 934575 5pages

Pawar S. M., Inamdar A. I., Gurav K. V., Chin S. W., Jo Y., Kim J., Im H. and Kim J. H., (2014), Growth of void free Cu_2ZnSnS_4 (CZTS) thin films by sulfurization of stucked metallic precursor films, *Vacuum*, **104** 57-60

Pawar S. M., Pawar B. S., Moholkar A. V., Choi D. S., Yun J. H, Moon J. H., Kolekar S. S. and Kim J. H., (2010), Single step electrosynthesis of Cu_2ZnSnS_4 (CZTS) thin films for solar cell application, *Electrochimica Acta*, **55** 4057-4061

Pourbaix M., (1974), Atlas of electrochemical equilibria in aqueous solution, *2nd ed*, *NACE Celebeor, USA*

Rahmani M. B., Keshmiri S. H., Shafici M., Latham K., Wlodaski W., Du Plessis J and Kalantar-Zadeh K., (2009), Transition from n to p-type of spray pyrolysis of deposited copper doped zinc oxide thin films for NO_2 sensing, *Sensor Letters*, **7**(4) 621-628

Scragg J. J., (2011), Copper Zinc Tin Sulfide thin films for photovoltaics: Synthesis and characterization by electrochemical methods, *Springer theses*, page 9-66

Scragg J. J., Dale P. J. and Peter L. M., (2008), Towards sustainable materials for solar energy conversion: preparation and photoelectrochemical characterization of Cu_2ZnSnS_4, *Electrochemistry Communications,* **10**(4) 639-642

Septina W., (2013), Studies on electrochemical synthesis of semiconductor thin films for photovoltaic applications, *Osaka University Knowledge Achive,* page 15

Septina W., Ikeda S., Kyoraiseki A., Itarada T., and Matsumara M**.,** (2013), Single-step electrodeposition of a microcrystalline $Cu_2ZnSnSe_4$ thin film with a kesterite structure, *ElectrochimicaActa,* **88** 436-442

Sheng C. Y., Jun Y. W., Rui L., Hua G. J., Xiao L. J., and Shi E. Y., (2014), Preparing Cu_2ZnSnS_4 films using the co-electrodeposition method with ionic liquids, *China Physics B,* **21**(5) **058801** 1-4

Shin S. W., Pawar S. M., Park C. Y., Yan J. H., Kim J. H. and Lee J. Y., (2011), Studies on Cu_2ZnSnS_4 (CZTS) absorber layer using different stacking orders in precursor thin films, *Solar Energy Materials& Solar Cells,* **95** 3202-3206

Shinde N. M., Dubal D. P., Dhawale D. S., Lokhande C. D., Kim J. H. and Moon J. H., (2012), Room temperature novel chemical synthesis of Cu_2ZnSnS_4 (CZTS) absorbing layer for photovoltaic application, *Materials Research Bulletin* **47** 302-307

[a]Shinde N. M., Deshmukh P. R., Patil S. V. and Lohhande C. D**.,** (2013), Aqueous chemical growth of $Cu_2ZnSnS4$ (CZTS) thin films: Air annealing and photoelectrochemical properties, *Materials Research Bulletin,* **48** 1760-1766

[b]Shinde N.M., Deokate R. J., and Lokhande C. D**.,** (2013), Properties of spray deposited Cu_2ZnSnS_4 (CZTS) thin films, *Journal of Analytical and Applied Pyrolysis*, **100** 12-16

Singh O. P., Muhunthan N., Singh N. V. and Singh B. P**.,** (2015), Effect of annealing time on the composition, microstructure and band gap of copper zinc tin sulfide thin films, *Research Article,* **6**(1) 2-7

Smits (1958), Measurement of sheet resistivity with the four point-probe. *Bell System Technical Journal*, **34,** 711-718

Song X., Ji X., Li M., Luo X. and ZhangH., (2014), A review on development prospect of CZTS Based Thin Film Solar Cell, *international Journal of Photoenergy,* Article ID 613173, 11pages

Tiong V. T., Bell J., and Wang H., (2014), One-step synthesis of high quality kesterite Cu_2ZnSnS_4 nanocrystals-a hydrothermal approach, *Beistein Journal of nanotechnology*, **5** 438-446

Tumuluri A., Naidu K. L., and Raju K. C. J., (2014), Band gap determination using Tauc's plot for $LiNbO_3$ thin films, I

Umar A., Akhtar S. M., Badran R. I., Abaker M., Kim S. H., Al-Hajri A. and Baskoutas S., (2013) Electrical properties of solution processed p-SnSnanosheets/n-TiO_2 heterojunctions assembly, *Applied Physics Letters* **103**-101602

Vasekar S. P. and Dhakal T. P., (2013), Thin film solar cells using Earth abundant materials, *in Tech open* 145-168

Wang H., (2011), Progress in thin film solar cells based on Cu_2ZnSnS_4, *International Journal of photoenergy*, Article ID 801292 10pages

Wang H. and Bell J. M., Thin film solar cells based on Cu_2ZnSnS_4 absorber. In the 5th World Congress on Engineering Asset Management (WCEAM 2010), 25-27 October 2010, *Brisbance Convention and Exhibition Centre*, Brisbance, Qld

Xie M., Zhuang D., Zhao M., Li B., Cao M and Song J., (2014), Fabrication of Cu2ZnSnS4 thin films using a ceramic quartenary target, *Vacuum* **101** 146-150

Yao M., Lin J., Liu M. and Xu Y., (2012), Detection of chromium in waste water from refuse incineration power plant near Poyang Lake by Laser induced breakdown spectroscopy, *Applied Optics,* **51(10)** 1552-1557

Zhou H., Hsu W., Duan H., Bob B., Yang W., Song T., Hsu C. and Yang Y., (2013), CZTS Nano crystals: a promising approach for next generation thin film photovoltaic, *Energy Environmental Science,* **6** 2822-2838